Enhancing searches for Supersymmetric-top pairs using Higgs tagging at 13 TeV

A Thesis

submitted to
Indian Institute of Science Education and Research Pune
in partial fulfillment of the requirements for the
BS-MS Dual Degree Programme

by

Shivani Lomte
Registration No. : 20151126

Indian Institute of Science Education and Research Pune
Dr. Homi Bhabha Road,
Pashan, Pune 411008, INDIA.

May, 2020

Supervisor: Dr. Seema Sharma

Certificate

This is to certify that this dissertation entitled **Enhancing searches for Supersymmetric-top pairs using Higgs tagging at 13 TeV** towards the partial fulfilment of the BS-MS dual degree programme at the Indian Institute of Science Education and Research, Pune represents study/work carried out by Shivani Lomte at Indian Institute of Science Education and Research under the supervision of Dr. Seema Sharma, Associate Professor, Department of Physics , during the academic year 2019-2020.

Shivani Lomte

Dr. Seema Sharma

Committee:

Dr. Seema Sharma

Prof. Monoranjan Guchait

This thesis is dedicated to my Parents

Declaration

I hereby declare that the matter embodied in the report entitled **Enhancing searches for Supersymmetric-top pairs using Higgs tagging at 13 TeV**, are the results of the work carried out by me at the Department of Physics, Indian Institute of Science Education and Research, Pune, under the supervision of Dr. Seema Sharma and the same has not been submitted elsewhere for any other degree.

Dr. Seema Sharma

Shivani Lomte

Acknowledgments

I would like to express my deepest gratitude to my project supervisor, Dr. Seema Sharma for her constant guidance over the past two years. It was her encouragement and continued support that kept me motivated throughout the project. Her extremely hardworking nature and taking up challenges was an inspiration for me. I would like to deeply thank Prof. Monoranjan Guchait for his extremely useful inputs and feedback, and interacting with him was a great learning experience. I want to express my gratitude to Dr. Aditee Rane for providing background samples and for her useful suggestions. I want to specially thank Bhumika Kansal for helping me right from the starting, with generating samples and debugging. I also would like to thank Shubham Pandey for providing useful suggestions and to Dr. Vinay Hegde for helping with Higgs Combine Tool. The weekly group meetings indeed helped me learn a lot of physics in a broader sense, thanks to the whole group including Niramay Gogate, Alpana Sirohi and Nukulsinh Parmar.

I want to express my gratitude to the IISER Pune EHEP group and the Physics department for the various interesting seminars which provided a great research environment. I also want to thank the IT department for their efforts in providing a working IISER CMS cluster. I thank the DST INSPIRE program for providing financial support.

A big thanks to my mom and dad for their love and support which kept me going, and to my brother who motivated me to work hard and never give up. Last but not the least, thanks to all my friends and the physics room gang for all the fun and interesting discussions over coffee breaks.

Contents

List of Figures

List of Tables

Abstract

Supersymmetry is one of the Beyond Standard Model theories which is postulated to resolve some of the gaps in the Standard Model. It predicts a partner particle for every SM particle and these new particles are expected to be massive. If they are accessible at the LHC, they can be produced in pp collisions and searching for these particles is one of the primary goals of the ATLAS and CMS experiment. There is a strong motivation to look for supersymmetric partner of the SM top quark, since its existence will help stabilize the divergent correction to Higgs mass where the maximum contribution comes from the massive top quark. There are existing analyses which search for particles in a variety of final state signatures. This thesis presents a search for pair produced stop quark in single lepton final state and in fully hadronic final state along with large missing transverse momentum and multiple b-jets.

This thesis targets a SUSY model which has a Higgs boson in the decay cascade of the pair produced stop particle ($\tilde{t_1} \rightarrow t\tilde{\chi_2^0}$ and $\tilde{\chi_2^0} \rightarrow H\tilde{\chi_1^0}$). This model is not extensively studied at the CMS experiment and can be an interesting channel to look for SUSY with Higgs boson in the final state. Kinematic variables are used to reduce background events and maintain signal events as much as possible. The mass spectra of the SUSY particles, which are free parameters of the theory determines the kinematics of the various particles in the event, including the Higgs boson. The Higgs particle is reconstructed in two categories, tagged and resolved for high and low momentum Higgs respectively. The performance of the analysis is studied with additional tagged Higgs as compared to the traditional baseline event selections. Limits are obtained at 95% confidence level as a function of the mass of stop for different model scenarios at luminosity $\mathscr{L} = 150$ fb^{-1} of simulated data at 13 TeV centre of mass energy in the CMS detector configuration.

Chapter 1

Introduction

Particle physics is the discipline which describes the elementary particles in the universe around us and how they interact with each other. Many of its predictions are tested in experiments to a good precision. The last missing piece of the Standard Model (SM), the Higgs boson was discovered in July 2012 by the CMS and ATLAS experiments. The SM has been a successful theory however, some important issues remain to be addressed like matter-antimatter asymmetry, dark matter, neutrino oscillations to name a few. It is believed that SM is only a part of a broader theory. Many particle physics theories are proposed which attempt to fill the gaps of the SM. One such theory is Supersymmetry (SUSY) which if found true, would address many of the unexplained phenomena in physics. This thesis presents a search for supersymmetric-top (stop) quarks which is one of the new particle predicted by SUSY. Here, we have targeted models where the cascade decay of stop quark involves a Higgs boson and an analysis is designed to tag the Higgs particle. We study the performance of this analysis in both single lepton and fully hadronic final state and reconstruct the Higgs particle in two categories, tagged and resolved depending on its momentum. There are not many searches with Higgs in cascade decay of stops and there exist SUSY parameter space where this model can be important to study. It is found that the Higgs tagging requirement improves single lepton analysis as opposed to only baseline selections. The inclusive search in fully hadronic channel has good sensitivity to our signal model and adding Higgs requirement adds only a small improvement.

1.1 Standard Model

The Standard Model (SM) is a theory which explains the physics of elementary particles by describing the interactions between the matter particles mediated by the carrier particles [1]. It is the most successful particle physics theory to date. It is based on quantum field theory which encapsulates quantum mechanics and special relativity in a single framework. It successfully models the Strong force, Weak force and Electromagnetic force whereas gravitation, the fourth fundamental force is not incorporated in the SM. The particle content of SM can be divided into fermions which are the matter particles and bosons which are the mediator particles. Figure 1.1 shows the particle content of the SM. These can be grouped into 3 categories, spin $\frac{1}{2}$, spin 1, and spin 0. There are six quarks and six leptons arranged in three successively heavier generations which form the spin $\frac{1}{2}$ fermions. There are identical particles for every elementary matter particle with an opposite electric charge which are called the anti-matter particles. Spin 1 particles are the gauge bosons namely the photon, gluons, Z^0, W^+, W^-. The photon and gluons are massless whereas the Z^0, W^+, W^- are massive [7]. The only spin 0 (scalar) particle in the SM is the Higgs boson with a non-zero mass. Every fermion and boson has a field associated to it and they can interact with one another which is explained by the SM.

Despite its tremendous success, the Standard Model is an incomplete theory. There are various motivations for a Beyond Standard Model (BSM) theory [2].

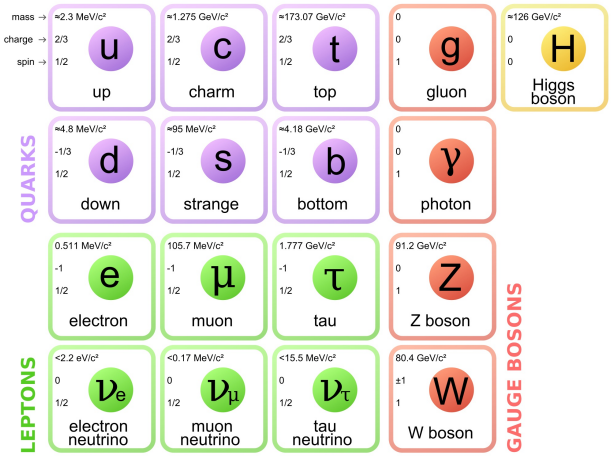

Figure 1.1: The Standard Model particle content. Source: [3]

1.2 Supersymmetry

Supersymmetry (SUSY) [4] is one of the most studied extension of SM which attempts to fill in the gaps of the SM. It proposes a partner particle for every SM particle with a spin difference of half-integer. Figure 1.2 shows the SM particles and their SUSY partners.

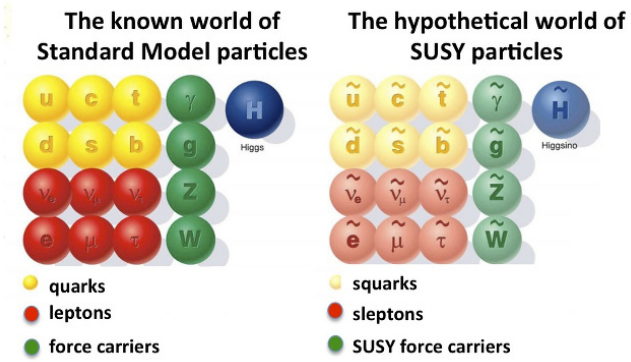

Figure 1.2: SM particles (left) and their SUSY partners (right). Source: [5]

One of the motivation for SUSY is that it addresses the Hierarchy Problem [6] which basically raises the question, why is there a huge gap between the electroweak scale (100 GeV) and Planck scale (10^{19} GeV), where quantum effects of gravity are expected to become important?

The mass of SM Higgs receives corrections from self-interactions, gauge loops and fermion loops and the highest contribution is from top quark as it is the heaviest particle in SM. These loop corrections are quadratically divergent and scale as Λ^2 for some cutoff scale Λ.

A Dirac fermion f having mass m_f coupling to the Higgs field adds a correction factor to m_H^2 as

$$\Delta m_H^2 = -\frac{|\lambda_f|^2}{8\pi^2}\Lambda_{UV}^2 + ... \tag{1.1}$$

whereas a boson coupled to the Higgs field adds a correction factor as

$$\Delta m_H^2 = +\frac{\lambda_b}{16\pi^2}\Lambda_{UV}^2 + ... \tag{1.2}$$

where Λ_{UV} is the ultraviolet cutoff. It is the scale at which we test for the new physics. If no new physics exists between the electroweak and Plank scale, then m_H^2 becomes infinitely large. However, the CMS (Compact Muon Solenoid) and ATLAS (A Toroidal LHC Apparatus) experiments at LHC (Large Hadron Collider) have observed the SM Higgs boson at a mass of 125 GeV [8, 9] which is finite. This means that there is a cancellation as the signs for the fermionic and bosonic corrections to m_H^2 are opposite. Figure 1.3 shows the Feynman diagram of the one-loop corrections due to fermion and boson to m_H^2 term. If for every fermion, we introduce an appropriate boson and vice versa, these quadratic corrections can be cancelled. This is exactly what SUSY does by postulating a symmetry between the fermions and bosons and this stabilizes the Higgs mass.

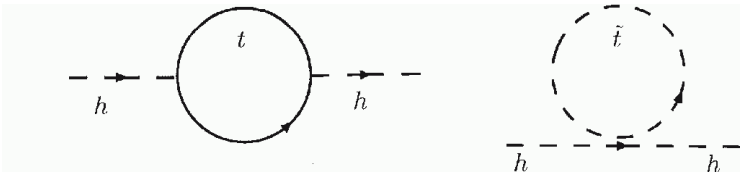

Figure 1.3: Correction to Higgs mass from top quark (left) and from stop quark (right). Source: [10]

This theory attempts to resolve the Hierarchy Problem and also has a potential dark matter particle candidate. It postulates that the SM particle and SUSY particle have all quantum numbers same except for their spin. This would imply the existence of selectron, superpartner of SM electron which would be a boson with the same mass and charge as the electron. However, we have not observed the selectron at the same mass as the electron. Thus, the theory is believed to have spontaneously broken symmetry which then allows the superpartner particles to have masses different from their SM particles. However, to avoid the fine tuning of the Higgs mass, the SUSY particles should have a mass not too different from their SM partners, so they could be accessible at the LHC energies.

1.3 Simplified Models

Introducing a supersymmetric particle for every SM particle generates unknown parameters like masses and their couplings to each other which decides the decay possibilities into other particles. SUSY does not predict these which gives rise to a large number of free parameters in

this theory. This makes it very challenging to explore all the possibilities in the experiment. Simplified Models [11, 12] have become quite popular which are built with the minimum number of particles required in order to reduce the number of free parameters. It is an approach where one can test for new particles and their decay probabilities instead of testing for full particle physics theories. The idea of simplified models is to present limits on very simple phenomenological models where each such model has very specific phenomenological features.

The model T1 postulates the existence of gluino and neutralino and has only two features, the mass of gluino and neutralino. The gluino is assumed to be heavier than the neutralino and the neutralino is assumed to be a stable particle. The gluino decays into the neutalino and a $q\bar{q}$ pair. The experimentalists at LHC then give an upper limit on the cross-section of this gluino pair production which is a function of the masses. Since the T1 model does not have large number of parameters, it is easier to set some constraints on this model. However, to cover a broader range of theoretical possibilities, a large number of different simplified models are considered where each model characterizes a single feature, usually in terms of particles participating in production processes, and decay branching fractions of particles produced. The limits on each such model can give us idea about the quantum of these features in the full theory.

An important motivation to search for stop ($\tilde{t}$) quarks is the fact that top quark has the largest fermionic contribution to the Higgs mass correction owing to its large mass. Thus $\tilde{t}$ quark which is a boson, will play a major role in stabilizing the Higgs mass, if it exists in nature. Several SUSY scenarios allow $\tilde{t}$ to be among the lightest sparticles [13] and have mass which is accessible at the LHC. Hence, the $\tilde{t}$ quarks are eagerly searched for at LHC. In SUSY models which conserve R-parity, the sparticles are always produced in pairs and the decay chain will end in one Lightest Supersymmetric Particle (LSP), which cannot decay further and hence is stable. Thus, if the lightest neutralino ($\tilde{\chi_1^0}$) is the LSP, then it is a good candidate for dark matter particle. Multiple searches have been done at the CMS and ATLAS experiment looking for pair production of $\tilde{t_1}$ quark. These searches have been pushing the limit on $\tilde{t_1}$ mass. The most recent searches [14] carried out by the CMS at 13 TeV and 137 fb^{-1} luminosity has pushed the mass limit to 1.2 TeV for the process $pp \rightarrow \tilde{t_1}\tilde{t_1^*}$, $\tilde{t_1} \rightarrow t\tilde{\chi_1^0}$.

1.4 Motivation for this thesis

The search for SUSY particles has been one of the primary goals of the LHC program. ATLAS and CMS experiments have designed dedicated search analyses to look for SUSY particles in pp collisions in various final state possibilities [15, 16]. These experiments have put stringent limits on the masses of gluions, squarks, and electroweak SUSY particles.

The limit on $\tilde{t_1}$ mass is increasing and several analyses are performed for the $\tilde{t_1} \rightarrow t\tilde{\chi_1^0}$ mode. For higher range of $\tilde{t_1}$ mass, $\tilde{t_1} \rightarrow t\tilde{\chi_2^0}$ mode is also important. There are regions in the parameter space where this decay mode is equally important. If the mass of $\tilde{\chi_2^0}$ is accessible at the current LHC energies, then $\tilde{\chi_2^0}$ can participate in the decay chain of $\tilde{t_1}$ and these models can be studied at the CMS.

The neutralinos are a linear combination of the gauginos (bino $\tilde{B}$ and wino $\tilde{W^0}$) and higgsinos ($\tilde{H_u^0}$ and $\tilde{H_d^0}$) [4]. The stop-top-neutalino coupling has two components, stop-top-gaugino and stop-top-higgsino where the latter component has a Yukawa coupling term which depends on the top quark mass. In such scenarios stop decay to higgsino-like neutralino becomes important due to the sizable Yukawa coupling. Note that higgsino-like charginos are also important, however since b-quark has mass an order of magnitude smaller than t-quark (Yukawa coupling has fermion mass term), we do not consider stop-bottom-chargino interactions in this thesis.

The stop-top-neutralino coupling will be larger for that neutralino which has a larger higgsino component in its linear combination. A larger coupling strength implies a larger branching ratio. Therefore, if $\tilde{\chi_2^0}$ has larger higgsino component than $\tilde{\chi_1^0}$, then $\tilde{t_1} - t - \tilde{\chi_2^0}$ coupling strength will be larger than $\tilde{t_1} - t - \tilde{\chi_1^0}$, which then implies that the BR for $\tilde{t_1} \rightarrow t\tilde{\chi_2^0}$ mode is larger than $\tilde{t_1} \rightarrow t\tilde{\chi_1^0}$ mode. This thesis targets such simplified models. It postulates the existence of $\tilde{t_1}$, $\tilde{\chi_1^0}$ and $\tilde{\chi_2^0}$ and it is assumed that $\tilde{t_1}$ can decay to only the two lightest neutralinos, $\tilde{\chi_1^0}$ and $\tilde{\chi_2^0}$ along with a t quark. Depending on the nature of $\tilde{\chi_2^0}$, it will decay to Higgs boson or Z boson or photon along with $\tilde{\chi_1^0}$. In this study, we have only considered $\tilde{\chi_2^0} \rightarrow H\tilde{\chi_1^0}$ decay mode. There are four parameters in this model, masses of the three sparticles and the branching ratio (BR) of $\tilde{t_1} \rightarrow t\tilde{\chi_2^0}$. The BR of $\tilde{t_1} \rightarrow t\tilde{\chi_1^0}$ will be 1 - BR($\tilde{t_1} \rightarrow t\tilde{\chi_2^0}$) since these are the only two allowed modes. These models are not extensively studied at LHC and it is an interesting channel to search for in the experiment. The ATLAS experiment has done a search for this model with Run 1 data and can be found at [17].

Chapter 2

Experimental setup and event reconstruction

2.1 Large Hadron Collider

At the European Center for Nuclear Research (CERN), large number of physicists and engineers probe the fundamental structure of our universe. The Large Hadron Collider (LHC) [18] is a 27 km circumference ring which collides proton beams at 13 TeV centre of mass energy in head-on collisions with a luminosity of $10^{34} cm^{-2} s^{-1}$. The beam energy and luminosity are chosen to study physics at TeV energy scale. This conditions requires for a detector with specific design. The general purpose detectors observe around 10^9 inelastic collision events per second. The rate of event selection should be reduced to about 100 events per second for permanent storage and subsequent analysis. The time between each bunch crossing is 25 ns which requires fast read-out and trigger systems. At the given luminosity, for every event of interest there are about 20-30 inelastic collisions which are superimposed. The interaction point of an interesting event can have particles from other interactions from the same bunch crossing. This requires that the response time of the detector elements and its electronic signals be compatible with it. Using high granularity detectors having good time resolution can reduce the effect of the pile-up. This requires a large number of detector channels and they all need to be extremely synchronized. A high level of radiation is also experienced by the detectors due to large flux of particles from interaction point which

requires radiation-hard detectors as well as the front-end electronics. CMS and ATLAS are two general purpose detectors which are at two of these locations and they are looking for signatures of new physics.

2.2 CMS Detector

The CMS detector [19] has a cylindrical geometry and has an onion-like layered structure where each layer is specialized to perform a particular function. It mainly consists of tracker, electromagnetic and hadronic calorimeter, superconducting magnets and muon detectors.

The main distinguishing feature of CMS is its high magnetic field solenoid, full silicon based tracker and a homogeneous scintillating crystal based electromagnetic calorimeter. The main task of the detectors is to identify the particles produced, measure their energy and momentum and then piece this information together to study the collision event.

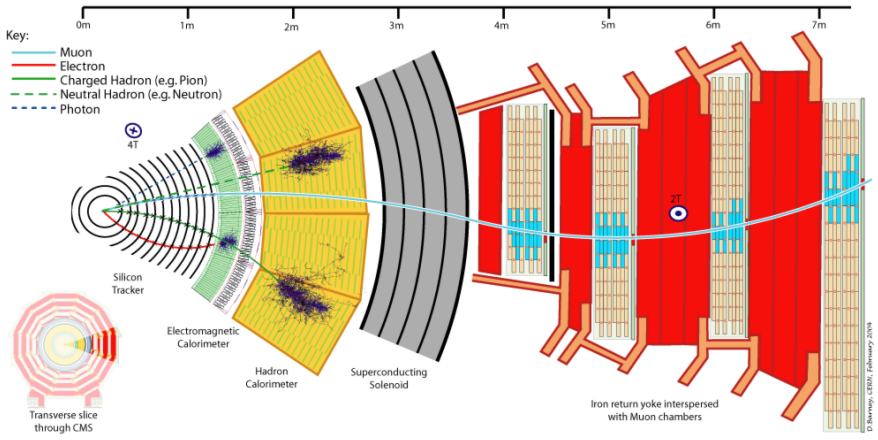

Figure 2.1: Transverse slice of the CMS detector. Source: [20]

The beam axis is taken as the z-axis, with x-axis pointing towards the centre of the ring and y-axis pointing in the vertical direction. The point where the p-p collision occurs is called the interaction point. The azimuthal angle ϕ is measured from x-axis in the x-y plane. The polar angle θ is measured from the z-axis and pseudorapidity is defined as η = - ln $\tan(\theta/2)$ which is usually used instead of θ.

Solenoid: The CMS has a 4 Tesla superconducting solenoid which is 13 m long and 6 m inner diameter. It uses Niobium-Titanium (NbTi) superconducting wire and is operated at few Kelvins. This enables very high currents though the solenoid which generates the large magnetic field which is used to bend the path of high momentum particles. There are physics processes which can give high energy particles which are of interest for new physics searches. To measure the momentum of such particles, we need strong magnetic fields which allows for a higher bending. The bore of the magnet coil accommodates the inner tracker and the calorimeters inside it. Electrons and photons shower and deposit their energy in ECal. However, muons do not undergo Bremsstrahlung and hence do not shower in the calorimeters which is why we can only measure the muon momentum, and for that we rely on the tracker and the muon chambers to get a good resolution.

Tracker: The aim of the tracker is to correctly identify the trajectories of charged particles produced in the collisions and precisely measure its momentum. 3 layers of silicon pixel detectors are placed close to the interaction point. This measures the impact parameter of charged particles and the position of secondary vertices which helps to identify heavy flavor particles like b-quarks. There are 10 layers of silicon microstrip detectors for granularity and precision purposes. In this busy environment, the electronics system need to have a good tolerance for the proper functioning of the detector. Silicon detectors are used which are designed to satisfy these requirements on granularity, fast response and radiation resistance. When a particle passes through the Silicon tracker, it interacts electromagnetically with the silicon and produces tiny electric signals which are called hits and these hits are used to identify the track of the particle. The tracker is made up of low atomic weight material which results in low energy losses when the particle produces hits in the detector. This is important for good momentum measurements. The tracker helps to reconstruct electrons, muons and charged hadrons.

Calorimeters: Energy measurement of the particles produced in the collision is extremely essential to understand the collision. This is achieved by two types of calorimeters, the Electromagnetic Calorimeter (ECAL) and the Hadronic Calorimeter (HCAL).

The **ECAL** is designed to measure the energy of electrons and photons by completely absorbing their energy. It is made up of lead tungstate crystals ($PbWO_4$) which is a scintil-

lating material i.e. it produces light when electrons or photons pass through it. The amount of light is proportional to the energy of the charged particle passing. Photodetectors are then used to detect this light and convert it into an electrical signal which can be further analyzed. The electrons in GeV energy range lose their energy by bremsstrahlung and the photons lose energy predominantly by pair production. This gives rise to secondary e^+e^- pairs and photons which develops into a shower. These secondary particles interact with the ECal material and deposit their energy. This enables the energy measurement of the primary electron or photon. This electromagnetic shower is characterized using radiation length and Moliere radius which is a feature of the nature of this radiation-matter interaction. The radiation length is defined as the longitudinal distance in which the primary electron loses 1/e of its initial energy. For photons, it is 7/9 of its free path distance of pair production. The Moliere radius is defined as the transverse distance wherein the electron loses 90% of its energy in an EM shower in a cylinder of Moliere radius. The ECAL is surrounded by a sampling hadron calorimeter (HCAL) with coverage upto $|\eta| < 3.0$.

The **HCAL** is designed to measure the energy of hadron jets. This works on the basis of nuclear interaction between the incoming particles and the detector material. When a high energy hadron passes through the HCAL, it interacts with the material and creates a spray of particles called a shower. The energy of these particles is deposited in the layers and measured. The hadronic shower can be characterized by interaction length (λ) which is defined as the longitudinal distance along the shower direction in which 67% of the secondary hadrons are absorbed by the detector material. The HCal comprises of layers of dense material (large atomic mass number) like brass and steel along with plastic scintillators. HCal is also designed to measure missing transverse momentum in the event. There are several interesting physics processes which can give large $\vec{p}_T^{miss}$ signatures and hence HCal plays a crucial role by fully containing the hadronic showers.

Muon Chamber: Muon detection is one of the major task of the CMS detector. There are physics motivations to look for muons in the final state. The CMS detector is designed to have precise and robust measurement of muon. The crucial features are muon identification, momentum measurement and triggering.

Trigger: The LHC experiences extremely high collision rates. The proton beam crossing

interval is 25 ns which corresponds to a crossing frequency of 40 MHz. For each bunch crossing, there are about 20 simultaneous pp collisions. This is an extremely huge amount of data and simply cannot be stored. A reduction in the event rate is extremely necessary which is done by the trigger systems in two steps. First is the Level-1 (L1) Trigger and second is the High-Level Trigger (HLT). The L1 Trigger makes a primitive selection and brings the event rate from 40 MHz to 100 kHz and the HLT further reduces the rate to few hundred Hz.

2.3 Event reconstruction

In a collision event, as the particles produced passes through the detector material, it interacts and deposits energy on its way [21]. This energy is converted into electronic signals and recorded for future analysis. This information is then used to interpret the passage of particles by meaningfully combining the information from the various sub-detectors and used for object reconstruction. The Particle Flow (PF) [22] algorithm developed by the CMS collaboration is used to identify and reconstruct the full event. It helps interpret the physics process that occurred in that collision event. The reconstructed particles include electrons, muons, photons, charged and neutral hadrons. The algorithm uses information from the tracker, ECAL, HCAL and muon detectors and gives PF candidate particles. The interaction of the various particle with the detector material is summarized in figure 2.2.

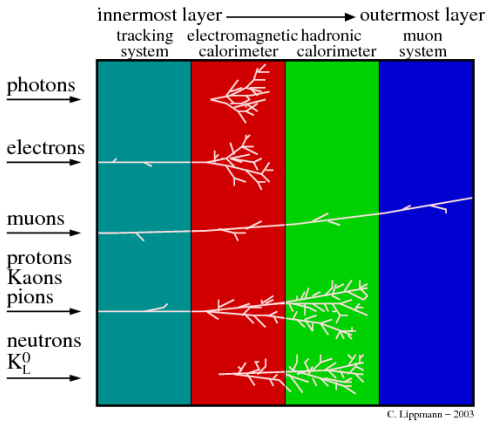

Figure 2.2: Schematic of particle signature in detector. Source: [23]

A charged particle passing through the Silicon tracker immersed in a magnetic field leaves

a trajectory in the form of 'hits' which the tracking algorithm uses to reconstruct a track. The curvature of the track is used to identify the charge and measure the momentum of the particle. Tracks are key ingredients for most of the particle reconstruction. It is very important for physics analysis to have good momentum resolution which then leads to good mass resolution.

After the tracker, the incoming particles interact with the calorimeters which are designed to stop the particles completely to measure their energy. This is done by completely absorbing their energy. Electrons and photons lose almost all of their energy by electromagnetic interaction in ECal. The hadrons deposit their energy in HCal by nuclear interaction. These hadrons can have both electromagnetic and hadronic components in their shower. The electromagnetic component is due to $\pi^0 \rightarrow \gamma\gamma$ decay where the photons undergo pair production and bremsstrahlung of electrons. The hadronic component of the shower deposit energy in both ECal and HCal before being fully absorbed.

In order to meaningfully reconstruct the various kinds of particles, the information from all the sub-detectors is optimally used as described below.

The LHC is a very busy hadronic environment where events containing isolated leptons mainly coming from W and Z decays are rare. However, these signatures are important for many new physics processes. This makes lepton identification very crucial for probing new physics phenomena [24].

Electron

Electrons interact with the ECAL through electromagnetic interaction and forms a shower of particles which deposits their energy in the ECAL. At energies of GeV scale, the dominant mode of energy loss is bremsstrahlung. These photons often convert to e^+e^- pair which in turn brems and a shower is developed. Electrons are reconstructed using combined information from the tracker and ECal.

Muon

Muons produced at CMS experiment have energies in GeV range and are thus minimum ionizing particles. They do not undergo bremsstrahlung and hence do not deposit much

energy in the calorimeters. It produces hits in the silicon trackers and the muon chambers and the combined information from these two is used to reconstruct muons. Tracks are first reconstructed independently in the inner tracker and the muon systems which are then geometrically matched. The hits are combined to reconstruct what is called a "global muon".

Photon

A photon, being a neutral particle does not give hits in the tracker. It interacts with ECal electromagnetically and deposits its energy. However, if the photon converts to e^+e^- in the tracker, then these can give hits in the tracker. In such cases, the electrons and photons have different cuts and criteria for identification.

Jets

A jet is a collection of particles which are produced from the hadronization of quarks and gluons. Since they carry color charge, they cannot exist freely in nature due to color confinement. These colored objects are reconstructed as jets in the detector. There are several algorithms designed to cluster the hadrons from the quarks and gluons.

Important aspects of the algorithm are infrared and collinear safety [25]. Infra-red safe jets are the ones which are not drastically influenced by the addition of soft gluons to the jet. A collinear safe jet is one which does not alter the contents of the jet upon splitting of a hard particle.

Sequential clustering algorithms cluster particles in the momentum space and are IRC safe. The CMS collaboration uses Anti$-k_T$ jets [26] which starts the clustering with high p_T particles and particles are sequentially added. This makes for the high resolving power of AK jets.

The AK algorithm uses the distance parameters d_{ij} and d_{iB} :

$$d_{ij} = min(p_{T_i}^{-2}, p_{T_j}^{-2}) \times \frac{\Delta_{ij}^2}{R_o^2} \tag{2.1a}$$

$$d_{iB} = p_{T_i}^{-2} \tag{2.1b}$$

For our analysis, we use AK jets of two radius parameters, $R_o = 0.4$ and 0.8 called AK4 and AK8 respectively. The AK8 jets are used to tag the Higgs bosons in the event. We use AK4 jets with $p_T \geq 30$ GeV and $|\eta| \leq 2.4$ and AK8 jets with $p_T \geq 200$ GeV and $|\eta| \leq 2.4$.

b-jets

Many exciting physics processes has b-quarks in the event. In our signal model of interest, there are top quarks which decay to b-quarks. Additionally, there are Higgs particles in the event whose dominant decay products are $b\bar{b}$ pair. Jets that originate from b-quark hadronization are called b-jets. It is essential to separate them from other light quark and gluon jets. The CMS collaboration has developed an algorithm to identify b-tagged jets [27]. The b-jets have a special feature which help to distinguish them from other lighter jets. The b-quark has a large mass around 4 GeV which gives its decay products high momentum. b-quarks hadronize to B-hadrons which are heavy and long-lived particles with a lifetime of the order of picoseconds. Thus they travel some distance (few mm) in the detector from the primary vertex before decaying to further particles. The point where they decay to further particles is called the secondary vertex which can be identified using the displaced tracks with the help of CMS tracker.

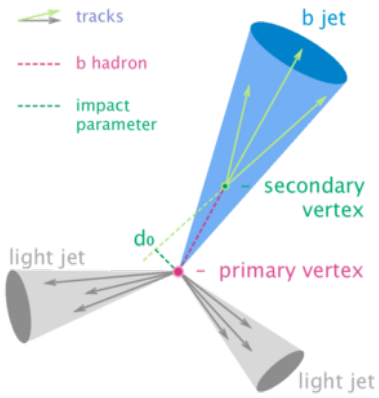

Figure 2.3: Schematic of b-jet tagging using secondary vertex. Source: [28]

Missing Transverse Energy

The presence of neutrinos and other weakly interacting particles in the event can be inferred by measuring a quantity called the Transverse Missing Energy (MET). It is a vector quantity defined as the negative of the vector sum of the transverse momenta of all the reconstructed particles in the event. The princilple of momentum conservation is used in the plane trans-

verse to the beam axis before and after the pp collision. Since the transverse momentum of the protons is zero before the collision, the sum of transverse momenta of all the particles in an event should add up to zero.

2.4 Simulation and event generation

A discovery in an analysis would be an excess of observed events over expected backgrounds in a designed search region. If an excess is observed, it needs to be compared with the theoretical prediction of a given model. Simulations of collision events are used to calculate the predicted signal event yields and the expected SM backgrounds. A high energy collision event can be generated and simulated using Monte Carlo (MC) softwares. These samples help understand the signal and background processes and also give an idea about the collider data collected in the experiments. These MC generators simulate processes occurring in proton-proton collisions and calculate their cross-section which depends on the model parameters like parton distribution function, coupling constants, masses of particles, branching ratios, etc. Madgraph [30] generates events and calculates the cross-section upto next-to-leading order (NLO) term. One can choose the model, the process, the center of mass energy, number of events, kinematic cuts on particles, etc while generating a physics process. Pythia [31] does the parton showering and hadronization of the process. Particles having a color charge like quarks and gluons cannot exist as free particles. They hadronize and create a shower of hadrons which are color-neutral. This shower of particles is called a jet which is modeled by Pythia. The interaction of these various particles with the detector is then simulated using Delphes [32].

Signal process

The model under study has four free parameters, the masses of the three SUSY particles and the decay probability (BR) of stop to decay via lightest or second lightest neutralino. We start with assuming a 50% BR for $\tilde{t_1} \to t\tilde{\chi_2^0}$ and 50% BR for $\tilde{t_1} \to t\tilde{\chi_1^0}$. Since there are two stops in the event, there are four possibilities for the stop-stop decay mode, i.e the two stops can decay via $\tilde{\chi_1^0}$-$\tilde{\chi_1^0}$, $\tilde{\chi_2^0}$-$\tilde{\chi_2^0}$, $\tilde{\chi_1^0}$-$\tilde{\chi_2^0}$, and $\tilde{\chi_2^0}$-$\tilde{\chi_1^0}$. This is shown in figure 2.4. Note that in the middle figure, either of the two stops can decay via $\tilde{\chi_1^0}$ and in this report, we will identify

both the scenarios as one. For 50% BR, the contribution of events from $\tilde{\chi}_1^0$-$\tilde{\chi}_1^0$ channel will be 25%, from $\tilde{\chi}_2^0$-$\tilde{\chi}_1^0$ will be 50% and from $\tilde{\chi}_2^0$-$\tilde{\chi}_2^0$ will be 25%. The three decay modes are separately generated and then added with the above weights using 'hadd' function in ROOT.

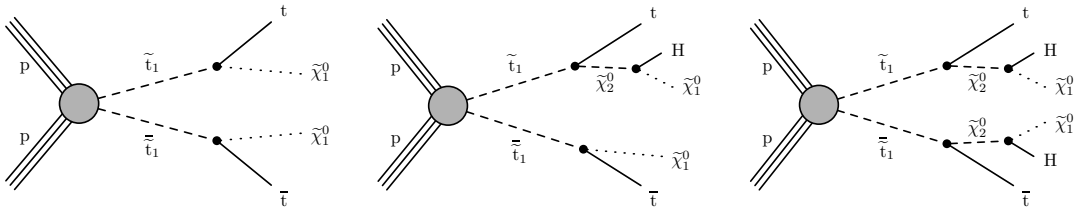

Figure 2.4: Feynman diagram for the signal models.

For the signal generation, MSSM_SLHA2 model is used. Madgraph5 is used for event generation, Pythia8 for hadronization and Delphes for detector simulation. Several mass points are generated to explore the different kinematic regimes. This can be changed in the parameter card in MadGraph. The cross-section for stop-stop production decreases with increasing mass of stop. Table 2.1 shows the mass of stop quark and the production cross-section (@ NLO) of stop quark pair. We have simulated signal process with stop mass ranging from 1.0 TeV to 1.3 TeV with 25 GeV difference. For each stop mass, there are multiple possible mass values for $\tilde{\chi}_2^0$ and $\tilde{\chi}_1^0$.

A large class of SUSY models exist and it is expected that pair production of strongly interacting SUSY particles like gluinos and squarks have the largest production cross-sections. The modes are:

$$pp \rightarrow \tilde{q}\tilde{g}, \tilde{g}\tilde{g}, \tilde{q}\tilde{q} \tag{2.2}$$

This thesis focuses on stop pair production and the SUSY particles other than the ones involved in our simplified model are assumed to be very heavy and not accessible at LHC and hence ignored for our model purposes.

$\tilde{t_1}$ mass [in TeV]	Cross-section [in fb]	$\tilde{t_1}$ mass [in TeV]	Cross-section [in fb]
1.000	6.83	1.175	2.01
1.025	5.7	1.185	1.88
1.050	4.76	1.200	1.70
1.075	3.99	1.225	1.44
1.100	3.35	1.250	1.22
1.125	2.82	1.275	1.04
1.140	2.54	1.300	0.887
1.150	2.38	1.350	0.646
1.165	2.15	1.400	0.473

Table 2.1: Mass of stop and cross-section for stop pair production process. Source: [29]

Background sources

In the Standard Model, there are several processes which have final state signature similar to signal process. These processes are called backgrounds. For the single lepton final state, the relevant backgrounds considered are:

- $t\bar{t} \to 1\ell$ process - this is a major background and it has a large cross-section.
- $t\bar{t} \to 2\ell$ process - if one of the two leptons is lost due to failing reconstruction or kinematic acceptance or isolation criteria. The lepton p_T then contributes to the missing momentum in the event which also mimics the signal kinematics of high $\vec{p}_T^{miss}$. Such an event can contribute to the signal region and the rate of such events is significantly high.
- $t\bar{t}H$ process where $t\bar{t} \to 1\ell$ - since the signal process has Higgs particle, this is also a SM background source.
- $t\bar{t}H$ process where $t\bar{t} \to 2\ell$ - if one of the two leptons is lost, this process can also contribute as background.
- $t\bar{t}Z$ process where $t\bar{t} \to 1\ell$ and $Z \to \nu\bar{\nu}$ - this process has a small cross-section but if the Z boson decays invisibly, this can contribute in high MET regions.

- $t\bar{t}Z$ process where $t\bar{t} \rightarrow 2\ell$ and $Z \rightarrow \nu\bar{\nu}$ - if Z decays invisibly and one of the two leptons is lost, this becomes a source of background.

Other backgrounds sources are not considered since the cross-sections are very small and most of the baseline selections might reject the background events.

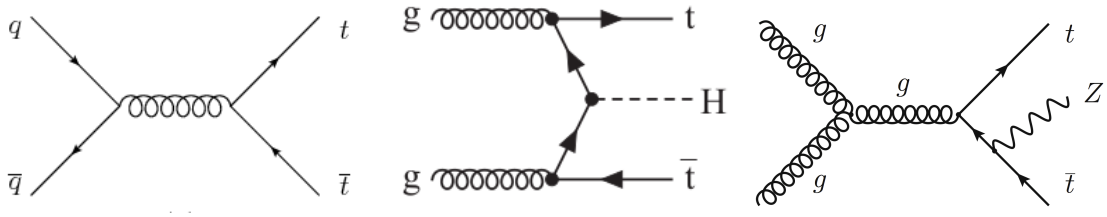

Figure 2.5: Representative feynman diagram for background processes in 1L channel.

The background processes are simulated using Monte Carlo simulations at center of mass energy of 13 TeV. MadGraph is used for event generation, Pythia for hadronisation and Delphes for CMS detector simulation. The processes are generated in two channels - semi-leptonic and dileptonic $t\bar{t}$ so as to have enough statistics (fully hadronic channel has BR around 45% and this fraction would be lost if we had generated inclusive samples). Table 2.2 lists the backgrounds, the cross-section of the decay channels and the number of MC events generated.

SM BGs	Channel	Cross-section [in pb]	N^{MC}_{events}
$t\bar{t}$	1ℓ	364.36	2M
$t\bar{t}$	2ℓ	87.31	2M
$t\bar{t}H$	$1\ell(t\bar{t})$	0.2231	0.5M
$t\bar{t}H$	$2\ell(t\bar{t})$	0.0558	0.5M
$t\bar{t}Z$	$1\ell(t\bar{t})\ \nu\bar{\nu}(Z)$	0.08712	50k
$t\bar{t}Z$	$2\ell(t\bar{t})\ \nu\bar{\nu}(Z)$	0.02178	50k

Table 2.2: SM backgrounds with decay channels with their cross-sections and number of MC generated events

Simulated events weight

The number of events of a process is calculated as the product of cross-section and integrated luminosity assuming unit acceptance and efficiency. This is the number of events observed in a physical process. However, it is not always feasible to generate this number in MC simulations. The stop pair production cross-section is of the order of femtobarns and at an integrated luminosity of 150 fb^{-1}, the number of events is of the order of a few thousand. This is too small a number to study the kinematics of the signal process. Hence a larger number of MC simulated events are generated (around 10^5) in this analysis. Similarly for $t\bar{t}H$ and $t\bar{t}Z$ SM processes, the physics number of events is small and hence a larger number of simulated events are generated.

However, the situation is reverse for the SM $t\bar{t}$ process. The number of events in the process is of the order of 10^7 and it is not computationally feasible to generate this large number of events. Hence few millions of events are generated which is good enough to study the kinematics. In order for the compare the kinematics of these processes, they need to be scaled to their production cross-section. Each event is weighted with a parameter called Evt_Wt which is the ratio of the physics number of events to the MC generated number of events,

$$Evt\_Wt = \frac{N^{phy}}{N^{MC}} = \frac{\sigma \times \mathscr{L}}{N^{MC}} \tag{2.3}$$

The production cross-section of the signal process is much lower than most of the SM backgrounds. Hence, we need to use event selections to reduce these backgrounds as much as possible while retaining most of the signal events.

Chapter 3

Analysis Strategy

3.1 Kinematics

The mass hierarchy of the SUSY particles determines the kinematics of the final state particles. Since we do not know the mass of the sparticles, we scan and study multiple mass values, and design a search strategy which has sensitivity to a range of mass spectra. The model assumes that $M(\tilde{t_1}) > M(\tilde{\chi_2^0}) > M(\tilde{\chi_1^0})$. If we fix mass value of $\tilde{t_1}$ and $\tilde{\chi_1^0}$, then there are huge number of possibilities for $\tilde{\chi_2^0}$ mass which has to lie in between $\tilde{t_1}$ and $\tilde{\chi_1^0}$ mass along with satisfying on-mass shell constraint for top and Higgs, i.e $M(\tilde{t_1})$-$M(\tilde{\chi_2^0}) \geq M(t)$ and $M(\tilde{\chi_2^0})$-$M(\tilde{\chi_1^0}) \geq M(H)$. Three scenarios are studied where $M(\tilde{\chi_2^0}) = x\ \Delta M(\tilde{t_1}, \tilde{\chi_1^0})$ with $x = 0.9$, 0.5 and 0.2. The first scenario (A) will give low p_T top quarks and high p_T Higgs bosons whereas the second scenario (B) will give intermediate p_T tops and Higgs and the third scenario (C) will give high p_T tops and low p_T Higgs. Figure 3.1 shows a schematic of the three scenarios where the vertical scale represents mass of the sparticle. Figure 3.2 shows the p_T of generator level top quark (left plot), $\tilde{\chi_2^0}$ (middle plot) and Higgs boson (right plot) for the three scenarios represented in three colors. The red plot in fig 3.2 left plot, the p_T distribution of top quark shows two peak like feature, one at large p_T value and one at small value. This is a manifestation of the two tops in the event coming via $\tilde{\chi_1^0}$ and $\tilde{\chi_2^0}$ each where $\Delta M(\tilde{t_1}, \tilde{\chi_2^0})$ is small but $\Delta M(\tilde{t_1}, \tilde{\chi_1^0})$ is large giving low and high p_T top quark. This effect is less visible as the two peaks merge when $\Delta M(\tilde{t_1}, \tilde{\chi_2^0})$ increases and is close to $\Delta M(\tilde{t_1}, \tilde{\chi_1^0})$ as seen for blue and magenta distributions. The middle plot shows that as we decrease $M(\tilde{\chi_2^0})$

while keeping M($\tilde{t_1}$) = 1.2 TeV and M($\tilde{\chi_1^0}$) $\tilde{1}$00 GeV, the p_T of $\tilde{\chi_2^0}$ increases as there is more energy available to boost t and $\tilde{\chi_2^0}$ as the energy needed to produce $\tilde{\chi_2^0}$ particle is decreasing. The opposite trend is seen for Higgs p_T (right plot) which depends on mass and p_T of $\tilde{\chi_2^0}$.

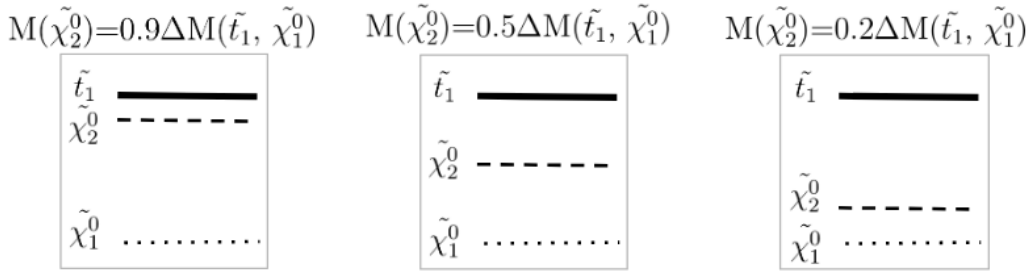

Figure 3.1: Schematic diagram for the mass hierarchy of the SUSY model particles

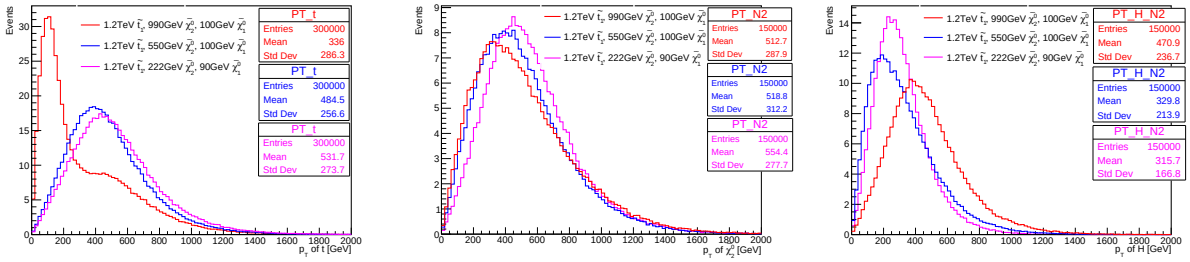

Figure 3.2: p_T of t-quark (left), $\tilde{\chi_2^0}$ (middle), and H (right) for the three scenarios $x = 0.9$ (red), 0.5 (blue), and 0.2 (magenta). For $x = 0.2$ case, the maximum kinematically allowed $\tilde{\chi_1^0}$ mass is around 95 GeV for on-shell condition, which is why the mass in the magenta case is taken as 90 GeV instead of 100 GeV which would have given exact comparisons.

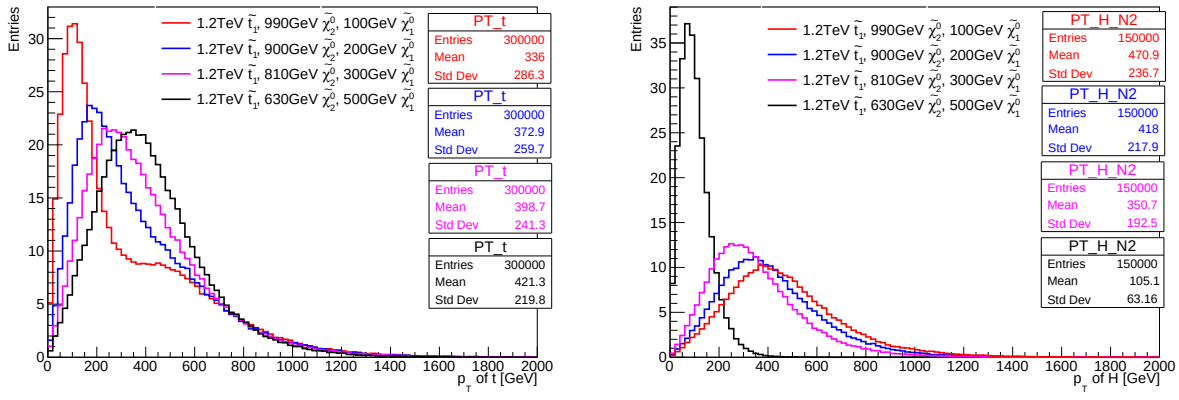

Figure 3.3: p_T of top quark and Higgs for models with $x = 0.9$ and fixing stop mass to 1.2 TeV and varying $\tilde{\chi_1^0}$ mass from 100 GeV to 500 GeV.

In a given model scenario (say x=0.9), on increasing $\tilde{\chi_1^0}$ mass for a fixed mass of $\tilde{t_1}$, the t p_T increases and H p_T decreases (see figure 3.3). In order to have maximum coverage of the parameter space, we reconstruct the Higgs particle in two categories to target high and low p_T Higgs. The first category targets boosted Higgs where the decay products are collimated which a standard jet clustering algorithm would reconstruct as a single jet called a Fat Jet. In order to have an Anti-k$_T$ jet with R-parameter 0.8, the Higgs particle should have $p_T \geq \frac{2M}{R_o}$ where $M = 125$ GeV and $R_o = 0.8$ giving $p_T \geq 300$ GeV. This gives an AK8 Higgs jet. Note that the event can also have boosted W or top jets for certain mass spectra of SUSY particles. Thus we impose a mass condition on the Fat Jet to lie in 100 - 150 GeV which is the Higgs mass window.

The second category is designed to target low p_T Higgs. In this thesis, only the $H \to b\bar{b}$ decay mode is studied which has a significant branching ratio of 58%. A di-jet pair both of which are tagged as having the B-meson is used to reconstruct the Higgs particle. There are two more b-tagged jets in the event coming from top-quark decays and it order to tag the b-jet pair from H decay, we impose a mass condition on the invariant mass of the b-tagged di-jet system to lie in 100 - 150 GeV. This jet is called as Resolved Higgs jet. Thus, the first category has high p_T Higgs reconstructed as Fat Jet and the second category has low p_T Higgs reconstructed as Resolved Jet.

With the current center of mass energy of 13 TeV, the LHC can produce highly boosted bosons and top quarks. However, perturbative and non-perturbative emissions from light-quarks and gluons also increase which can broaden and shift the mass peak of reconstructed jets. In such scenarios, jet substructure techniques can identify boosted hadronically decaying objects of interest. These algorithms can distinguish between jets originating from boosted bosons or top quarks and jets from light quarks or gluons. This uses the energy pattern of the jets which is different for QCD jets and boosted hadronic jets.

3.2 Soft Drop Mass Tagger

Soft Drop [36] is a jet substructure technique which is designed to remove wide-angled and soft radiation from a jet. Given a jet j, the last step of the jet clustering algorithm is undone and two protojets j_1 and j_2 are obtained. If j_1 and j_2 satisfies the Soft Drop condition, then

j is said to be the Soft Drop (SD) tagged jet.

SD condition:

$$\frac{min(p_{T_1}, p_{T_2})}{p_{T_1} + p_{T_2}} > z_{cut}(\frac{\Delta R_{12}}{R_o})^{\beta} \tag{3.1}$$

If not, then j is redefined to be j_1 and the procedure is repeated. If j is a single constituent such that it can no longer be declustered, then j is removed from the list. The parameter values chosen are $z_{cut} = 0.1$ and $\beta = 0.0$ which are used at CMS experiment.

Figure 3.4 shows the Fat Jet mass distribution before and after applying SD mass tagging for two signal model scenarios with high and low p_T Higgs boson. For model with M($\tilde{t_1}$)=1 TeV and large $\Delta M(\tilde{\chi_2^0}, \tilde{\chi_1^0})$, the Higgs is boosted and one of the two tops in the event is also boosted giving three mass peaks, at W mass, Higgs mass and top mass (fig 3.4 left plot). However, for models with M($\tilde{t_1}$)=1 TeV but small $\Delta M(\tilde{\chi_2^0}, \tilde{\chi_1^0})$, the Higgs has low p_T and both the tops are boosted, thus giving mass peaks at only W and top mass (3.4 right plot).

After applying SD mass condition on the Fat Jets, there is improvement in the resolution of the mass peaks. UE and pileup usually enhances the jet mass which after applying SD gets reduced to very low jet mass (peak near zero in Fat Jet mass distribution in blue).

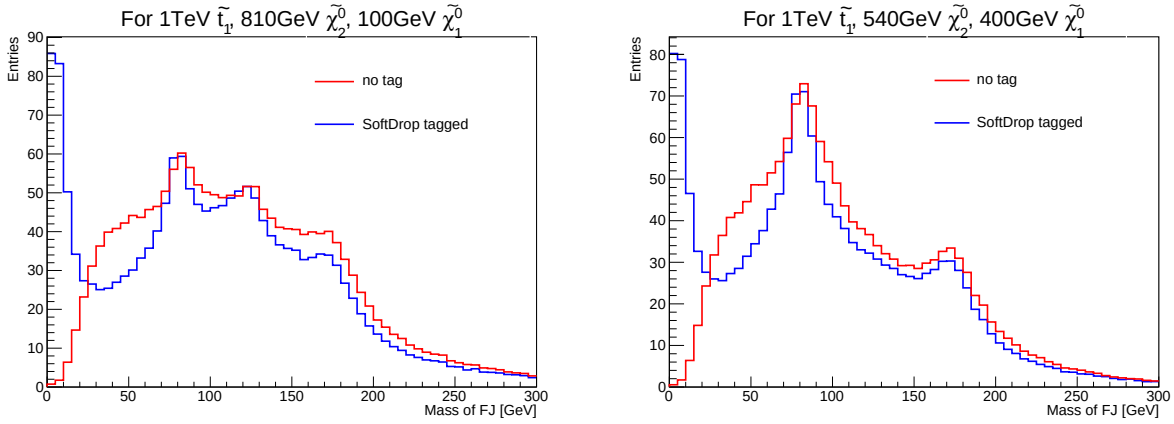

Figure 3.4: Fat Jet mass distribution before (red) and after (blue) applying SoftDrop tagger for signal model with large $\Delta M(\tilde{\chi_2^0}, \tilde{\chi_1^0})$ (left plot) and small $\Delta M(\tilde{\chi_2^0}, \tilde{\chi_1^0})$ (right).

3.3 N-subjettiness

This variable [37] is designed to count the prongness of a given jet. It is defined as

$$\tau_N = \frac{1}{d_o} \sum_k p_{T,k} \; min\{\Delta R_{1,k}, \Delta R_{2,k}, ..., \Delta R_{N,k}\} \tag{3.2a}$$

$$d_o = \sum_k p_{T,k} \; R_o \tag{3.2b}$$

where k goes over the constituents of the given jet and $p_{T,k}$ is their transverse momentum. $\Delta R_{J,k} = \sqrt{(\Delta\eta)^2 + (\Delta\phi)^2}$ is defined as the distance between subjet J and constituent particle k in the $\eta - \phi$ plane and R_o is the jet radius. This variable is used to find the number of subjets in a given jet. If the value of τ_N is very small (close to 0), then all the jet radiation is along the candidate subjet axes and the given jet has N or fewer subjets. However, if the value of τ_N is large (close to 1), then most of the energy is distributed away from the candidate subjet axes, implying that the jet has atleast N+1 subjets. One would expect τ_2 value for $W/Z/H$ jets to be small compared to QCD jets, however, QCD jets with large τ_1 value can have large τ_2 values, which makes the variable τ_N not a good discriminating variable. A preferred variable is the ratio of these two, τ_2/τ_1 which is also denoted as τ_{21}. This variable has better discriminating power and can be used to identify 2-prong jets.

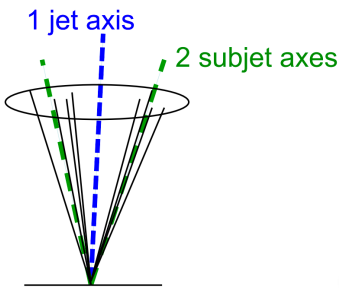

Figure 3.5: Schematic showing the two subjets of a 2-prong jet decay.

The $t\bar{t}$ background can have boosted W which is also a 2-prong decay. The variable τ_{21} can not distinguish between these W Fat Jet and H Fat Jet from the signal. It is only effective in reducing QCD jets contamination. To reduce W Fat Jet contribution, we use the p_T and η variable of the Fat Jet. This is shown in section 4.2 Higgs tagging.

Chapter 4

Stop search in single lepton channel using Higgs tagging

The presence of a single lepton, either electron or muon in the event provides a clean signature in the detector which is also easy to model in Delphes simulation. This section describes the search of stop quark in events with single lepton channel. The signal event has 2 tops and 0, 1 or 2 Higgs particles based on the decay mode of stop. The decay modes of $t\bar{t}$ are fully hadronic, semi leptonic and dileptonic modes. The left plot in figure 4.1 shows the decay modes and branching ratios of $t\bar{t}$ process where single lepton channel has BR of 45% and fully hadronic channel has BR of 46%. The branching ratio of Higgs to $b\bar{b}$ mode is around 58%.

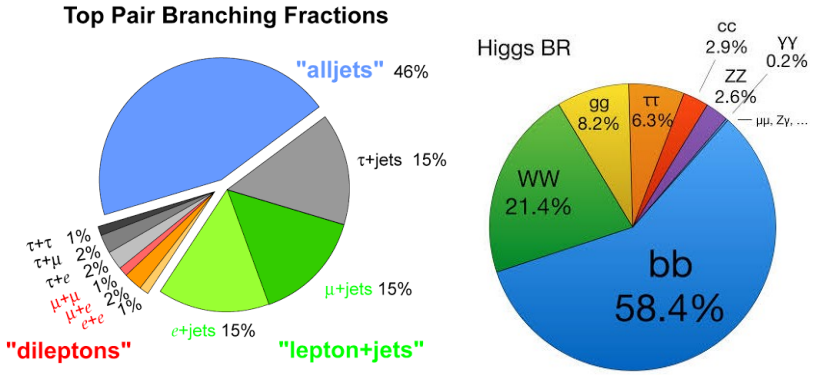

Figure 4.1: Decay modes and Branching Ratio (BR) of $t\bar{t}$ (left) and Higgs (right) decay. Source: [38, 39].

The top quark almost always decay to a bottom quark and a W boson, giving us 2 b-jets from the 2 tops each. The dominant decay mode of Higgs is $H \to b\bar{b}$ which results in large number of b-jets in the event. This selection can be helpful in extracting signal events.

4.1 Event selection

Kinematic distributions are studied to understand the signal and background processes and to exploit the differences between them in order to reduce the background contribution in the signal regions.

Table 4.1 shows the reconstructed objects and the selection cuts used. In Delphes, a jet is tagged as a b-jet if the value of b-tag==1 for that jet. This is done using a ΔR matching to a b-quark.

Object	Selection
Electron (e)	$p_T \geq 20$ GeV, $\eta \leq 2.5$
Muon (μ)	$p_T \geq 20$ GeV, $\eta \leq 2.4$
AK4 jets	$p_T \geq 30$ GeV, $\eta \leq 2.4$
b-tagged AK4 jets	$p_T \geq 30$ GeV, $\eta \leq 2.4$, b-tag=1

Table 4.1: Reconstructed object selection

One of the classic discriminating variable for searches with neutalinos is the missing transverse momentum ($|\vec{p}_T^{miss}|$ or MET) signature. It is defined as the magnitude of the negative of the vector sum of p_T of all the visible particles in the event.

$$MET = |\vec{p}_T^{miss}| = | - \sum_{i=vis} \vec{p_T}^{\,i}| \tag{4.1}$$

The true source of MET in the signal event comes from neutrinos from leptonic decay of top quark and from the LSPs whereas for the backgrounds the true source of MET is only neutrinos. If the LSPs have considerable boost and particular angular topology, these signal events can have significantly large values of MET as compared to the background events. The top row in figure 4.4 shows the MET distribution of the various backgrounds and two signal points. The tail in MET distribution suggests that we can look for SUSY signal in

the high MET regions since backgrounds have smaller contribution to high MET. A loose MET cut of 120 GeV is applied on the events which reduces some of the background events and retains most of the signal events.

The next classic signature for single lepton channels is high M_T values. For events where lepton is from a W decay, there also exist an associated neutrino. For the background processes, this is the only true source of MET and hence there is a correlation between the MET and the lepton p_T. This feature can be exploited by the M_T variable. It is defined as

$$M_T = \sqrt{2p_{T,\ell}\ p_T^{miss}\ (1 - cos(\Delta\phi(\vec{p}_{T,\ell}, \vec{p}_T^{miss})))} \tag{4.2}$$

where $p_{T,l}$ is the transverse energy of lepton, p_T^{miss} is missing transverse energy and $\Delta\phi(\vec{p}_{T,\ell}, \vec{p}_T^{miss})$ is the azimuthal angle between the lepton and MET. However, for the signal, there exist LSPs in the event which also contributes to the MET along with the neutrinos. Thus, the MET and lepton p_T will not have the same correlation as the background. M_T has a sharp fall at W mass value (around 80 GeV) for the background processes, however due to smearing, this can reach until 100 GeV and CMS paper [14] uses 150 GeV M_T cut. It is observed that this is indeed a good selection to reduce single lepton background events and keep most of the signal event.

The dominant background that passes high M_T selection and $N_\ell = 1$ is $t\bar{t} \to 2\ell$ process where one of the two leptons is "lost". This can happen due to failure in reconstruction or acceptance failure (p_T or $|\eta|$ outside the detector acceptance) or due to failure in isolation. Such events can be further reduced by demanding that the angle $\Delta\phi(J_{1,2}, \vec{p}_T^{miss})$ in the azimuthal plane between $\vec{p}_T^{miss}$ and the direction of the closest of the two leading jets (J_1 and J_2) be greater than 0.8. The $t\bar{t} \to 2\ell$ background process can have high p_T tops which makes the jets in the event collinear giving small $\Delta\phi$ values. This selection does not reduce the $t\bar{t}$ dilepton background by much. Another possibility is that the W boson in the event from top decay decays to a τ lepton which then decays hadronically. Such an event would give a hadronic signature even if the W decay was leptonic. Hence we need to study the contribution of such events which is discussed below.

We also studied the H_T distribution after applying the rest of the baseline selections and observed that a small amount of background can be reduced without reducing much of

signal. H_T is defined as the scalar sum of transverse momenta of the jets in the event (see figure 4.4).

$$H_T = \sum_j p_T^j \tag{4.3}$$

where j runs over all the jets in the event. $H_T \geq 500$ GeV selection is applied on the events.

Then, we have NJets ≥ 5 and NbJets ≥ 2 cuts to further reduce the background events. Table 4.2 shows a summary of the kinematic variables and cuts used for event selection.

Kinematic variable	Selection cut
N_ℓ	$= 1$
$\lvert\vec{p}_T^{miss}\rvert$	≥ 120 GeV
M_T	≥ 150 GeV
N_J	≥ 5
N_{bJ}	≥ 2
H_T	≥ 500 GeV
$\Delta\phi$ (J_{12}, $\vec{p}_T^{miss}$)	> 0.8

Table 4.2: Baseline selections for single lepton analysis

Figure 4.4 shows kinematic variables after applying baseline selections. A cutflow of the effect of these successive selections is shown in table 4.3. Table 4.4 shows the efficiencies of the baseline selections. The number of events survived after the selection (shown in percentage) is scaled to number of events without any selection (first row).

The events are further categorized by 'binning' in MET, N_J and N_{bJ} as :

- MET: [120-260], [260-380], [≥380] in GeV
- N_J: [5-6], [7-8], [≥9]
- N_{bJ}: [2], [≥3]

This gives us a total of 18 search bins. Multidimensional binning in these variables improves the sensitivity of the analysis to various signal scenarios as different models fall in different kinematic regions. This is also done for the fully hadronic analysis which is an inclusive one and is found to enhance the sensitivity of the analysis.

Selection	$t\bar{t} \to 1\ell$	$t\bar{t} \to 2\ell$	$t\bar{t}H \to 1\ell$	$t\bar{t}H \to 2\ell$	$t\bar{t}Z \to 1\ell$	$t\bar{t}Z \to 2\ell$	Total Bkg
No cut	55505100	13364800	33382	8346	13074	3268	68927970
$N_\ell = 1$	20532500	6139680	11792	3787	4932	1551	26694241
$MET \geq$120 GeV	1783750	910540	2077	972	2434	687	2700460
$M_T \geq$150 GeV	17981	361468	144	360	1041	370	381364
$N_J \geq$5	8963	32782	88	145	279	40	42297
$N_{bJ} \geq$2	4618	16423	49	103	133	20	21346
$H_T \geq$500 GeV	4427	12586	46	85	98	16	17257
$\Delta\phi(J_{12}, p_T^{miss}) \geq$0.8	1667	7465	20	48	81	12	9294

Table 4.3: Cutflow table for sequential event selections in single lepton analysis

Selection	$t\bar{t} \to 1\ell$	$t\bar{t} \to 2\ell$	$t\bar{t}H \to 1\ell$	$t\bar{t}H \to 2\ell$	$t\bar{t}Z \to 1\ell$	$t\bar{t}Z \to 2\ell$	Total Bkg
No cut	100	100	100	100	100	100	100
$N_\ell = 1$	37	46	35	45	38	47	39
$MET \geq$120 GeV	3.2	6.8	6.2	12	19	21	3.9
$M_T \geq$150 GeV	0.03	2.7	0.43	4.3	8.0	11	0.55
$N_J \geq$5	0.02	0.24	0.26	1.7	2.1	1.2	0.06
$N_{bJ} \geq$2	0.008	0.12	0.15	1.2	1.0	0.63	0.03
$H_T \geq$500 GeV	0.008	0.09	0.14	1.0	0.75	0.48	0.02
$\Delta\phi(J_{12}, p_T^{miss}) \geq$0.8	0.003	0.06	0.06	0.58	0.62	0.36	0.01

Table 4.4: Cutflow table for sequential event selections in single lepton analysis. The numbers show the events survived with respect to no selection.

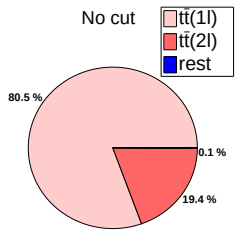

(a) N_{evts}^{tot}=68927970

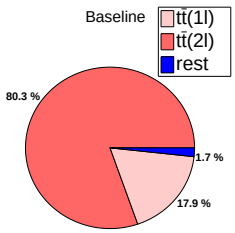

(b) N_{evts}^{tot}=9294

Figure 4.2: Background composition before and after baseline selections.

Figure 4.2 shows the background composition with no selections applied (left plot) and after applying baseline selections (right plot). Since the major contribution is from semi

leptonic and dileptonic $t\bar{t}$ process and the other backgrounds have very small cross-section, they are combined and marked as 'rest' in the pie charts. It is found that before applying event selections, the major background contribution is from semi-leptonic $t\bar{t}$ process sue to its highest branching ratio. However, after applying baseline selections, the contribution of semi leptonic $t\bar{t}$ process reduces, especially due to the M_T selection and the dominant contribution is from dileptonic $t\bar{t}$ process.

The effect of the various selections step-by-step on the background composition is shown in figure 4.3 starting with no selection to baseline selections. The effect of M_T can be seen in figure 4.3 (top right) where the semi-leptonic contribution is significantly reduced.

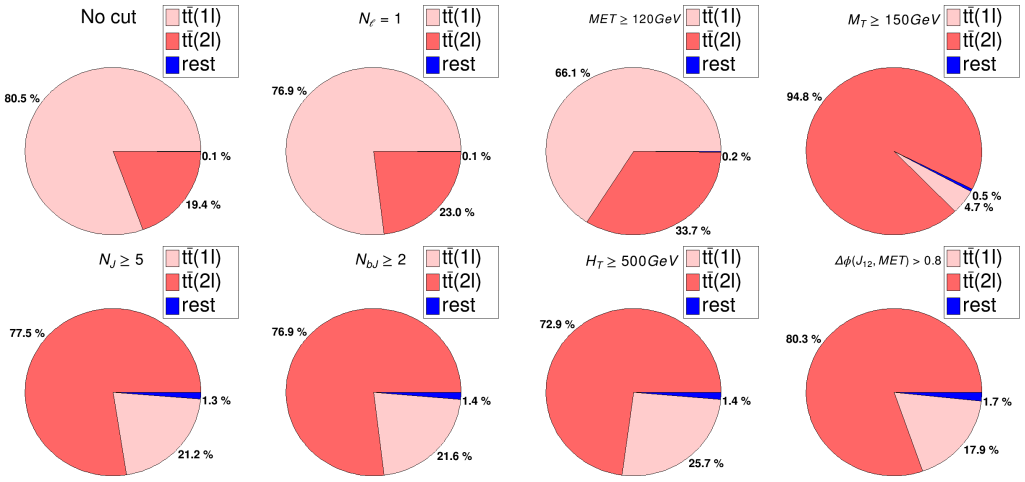

Figure 4.3: Pie chart showing background composition with sequential baseline selections.

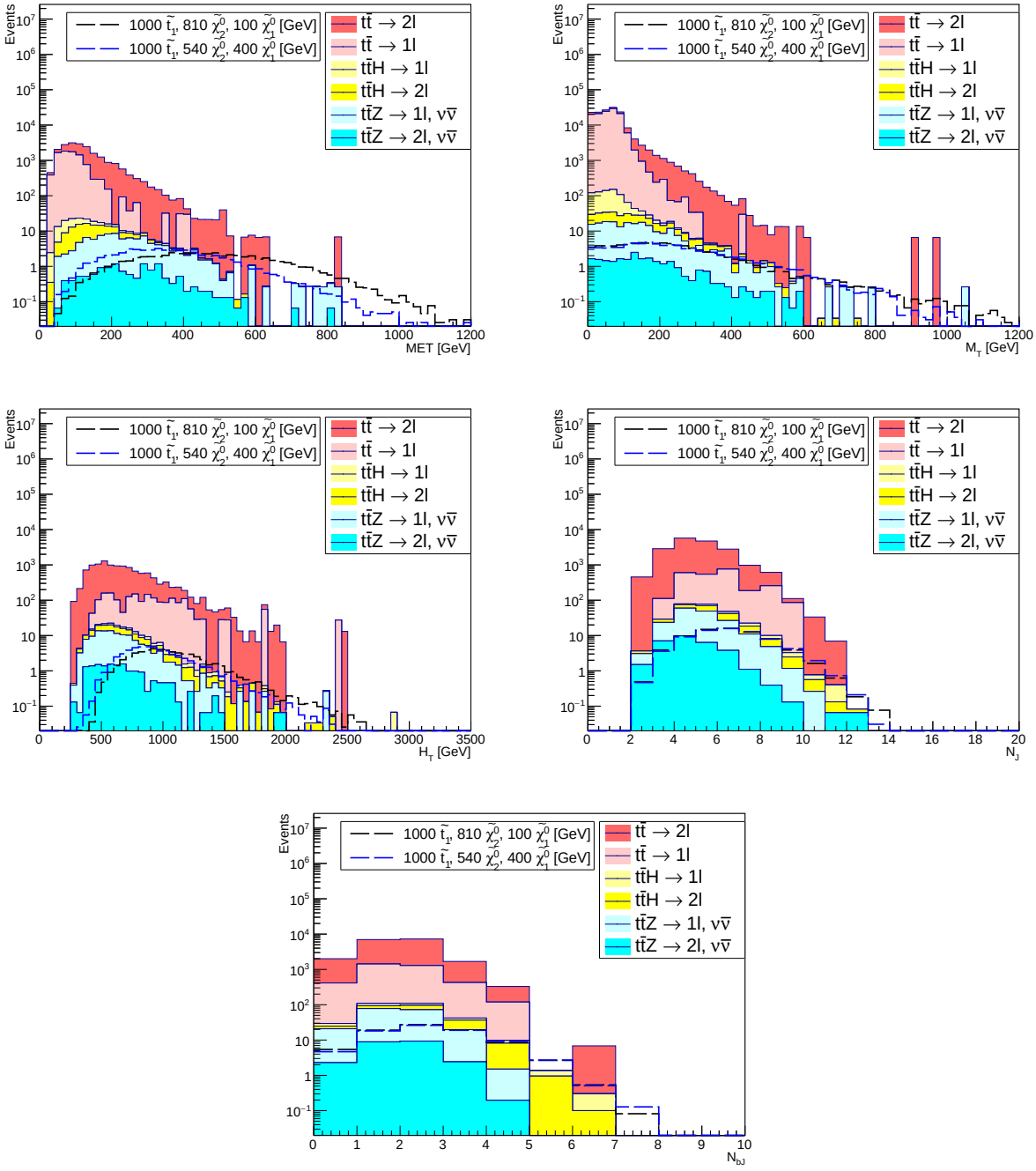

Figure 4.4: Kinematic distributions after applying baseline selections except that particular selection (also called N-1 selection). BS: $1\ell + MET \geq 120GeV + M_T \geq 150GeV + H_T \geq 500GeV + N_J \geq 5 + N_{bJ} \geq 2 + \Delta\phi(J_{12}, MET) > 0.8$

4.2 Higgs tagging

The mass spectrum of SUSY particles determine the kinematics of the event as is described in Section 3.1. The Higgs particle in the event is reconstructed in two categories depending on its transverse momentum. The first category targets the high p_T Higgs where it is reconstructed as a single Fat Jet. If such a jet is not found in the event, we look for a Resolved $b\bar{b}$ jet. A schematic of the two scenarios is shown in fig. 4.5.

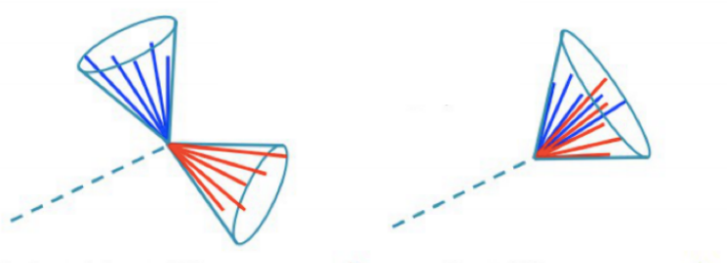

Figure 4.5: Schematic for Resolved (left) and Fat Higgs Jet (right). Source: [40]

Fat Jet category: Fat Jet is defined as the jet clustered using the Anti-k_T algorithm with R-parameter 0.8 and having a p_T cut of 200 GeV. Jet sub-structure techniques are used to tag the Higgs jets from the Fat Jets collection. The first variable to tag the Higgs jet is the jet mass, however there can be soft and wide-angled radiation contamination from QCD jets. Due to this effect, gluon or light-quark jets can get high mass and fall in the Higgs mass window. The contribution from such jets can be reduced by using Soft Drop mass tagger, described in section 3.2 which shows an improvement in distinguishing on the basis of jet mass. Figure 4.6 and 4.7 shows the Fat Jet mass distribution before and after applying baseline event selections respectively. The effect of the various tagging variables is studied for signal models with high (left plot) and low (right plot) p_T Higgs. On applying SD, the QCD jet mass distribution is pushed to close to zero (red plot), thus reducing contamination in signal regions. Next, to tag Higgs jet, the relation between p_T and R-parameter of the Fat Jet is used, which states that in order to have Higgs decay products in a single jet of R=0.8, the Fat Jet p_T should satisfy,

$$p_T \geq \frac{2 \times M_H}{R} \tag{4.4}$$

where $M_H = 125$ GeV and $R = 0.8$, giving $p_T \approx 312$ GeV. Thus, we apply a selection of

$p_T \geq 300$ GeV and $|\eta| \leq 2.4$ on the Fat Jet. This reduces contribution from W-jets which require a $p_T \geq 200$ GeV to form a Fat Jet (magenta plot). Next, we study the effect of N-subjettiness variable τ_{21} on Fat Jet. This helps in indentifying the number of subjets in the jet. Since there are boosted W bosons in the event, this variable does not distinguish between H and W jets since both have 2-prong decay structures, and hence isn't a good discriminating variable between H and W jets. However it does reduce contamination from QCD jets. This can be seen from the black plot which show the Fat Jet mass after τ_{21}<0.6. The peak at low mass values in red plot is of QCD jets after SD applied on them and after applying a τ_{21} cut, these events are significantly reduced as they do not pass the 2-prongness selection.

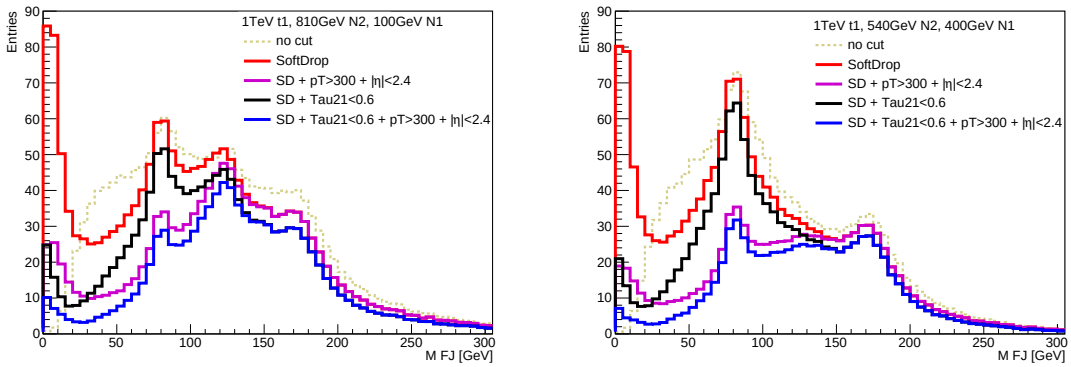

Figure 4.6: Fat Jet mass distribution before applying baseline selections showing the effect of various sub-structure selections. Model with large $\Delta M(\tilde{\chi}_2^0, \tilde{\chi}_1^0)$ giving high p_T Higgs (left plot) and small $\Delta M(\tilde{\chi}_2^0, \tilde{\chi}_1^0)$ giving low p_T Higgs (right plot) is shown.

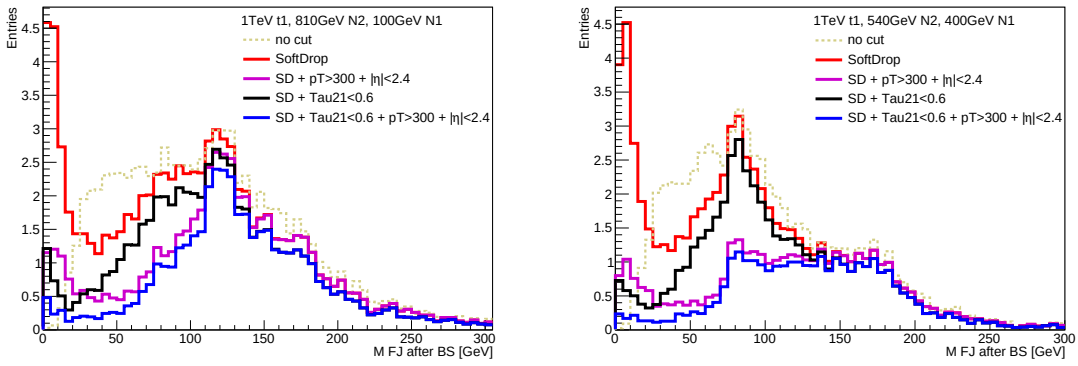

Figure 4.7: Fat Jet mass distribution after applying baseline selections showing the effect of various sub-structure selections. Model with large $\Delta M(\tilde{\chi}_2^0, \tilde{\chi}_1^0)$ giving high p_T Higgs (left plot) and small $\Delta M(\tilde{\chi}_2^0, \tilde{\chi}_1^0)$ giving low p_T Higgs (right plot) is shown.

Figure 4.8 shows the mass distribution of Fat Jet after matching to gen level particles to check for purity of the tagging method. This is done for models with high (left plot) and low (right plot) p_T Higgs model. The light pink is of SD tagged Fat Jet to have a reference for comparison. The red plot is for Fat Jet matched with gen level H and magenta plot for matching with gen level W. The two subjets of the Fat Jet are accessed and checked if they match to the b-quarks from H decay and if a matching is found, the mass of such a Fat Jet is plotted in blue. If a Fat Jet does not find a match with either of H or W or t, its mass is plotted in black. For models with low p_T Higgs where H is not reconstructed in a Fat Jet (right plot), there is no H peak and hence no match to gen level H or b-quarks is found. The matching is done using a ΔR of 0.4.

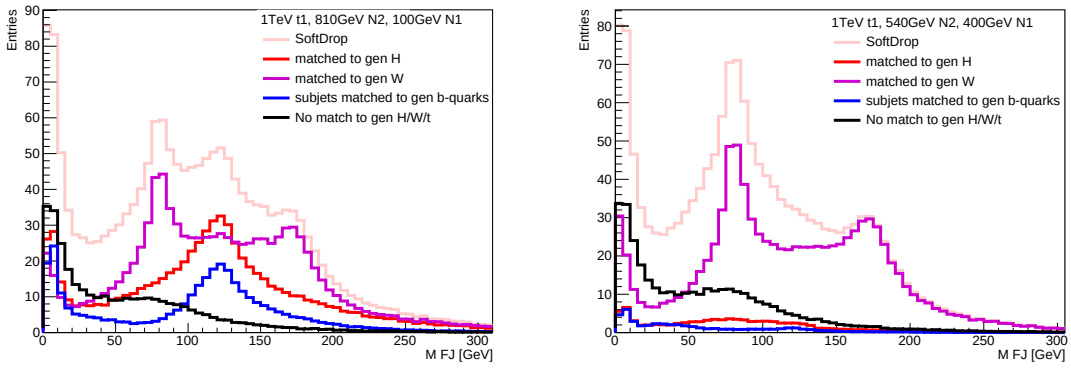

Figure 4.8: Fat Jet mass distribution when matched to gen level H (red), W (magenta), the two subjets of Fat Jet matched to b-quarks from H decay (blue) and when no matching t or H or W found (black). The matching is done using $\Delta R < 0.4$.

Resolved Jet category: If the Higgs particle has low or moderate transverse momentum, the decay products can't be reconstructed into a single AK8 jet. For such scenarios, we use AK4 jets which are tagged as b-jets and reconstruct the Higgs jet by 4-vector addition of all possible combination of two b-jets and a mass cut of 100 - 150 GeV is applied to ensure that the mother is a Higgs particle. Such a jet is called a Resolved Jet. A schematic is shown in fig. 4.5 (left) where the two small jets are AK4 b-tagged jets.

Figure 4.9 shows the invariant mass distribution of b-jet pairs for high (left plot) and low (right) p_T Higgs models before applying baseline selections and figure 4.10 shows the same after applying baseline selections. The black curve is for Resolved Jet candidates whereas the blue curve is for events in which the Resolved Jet is matched to generator level Higgs

particle in a ΔR of 0.4. This shows the purity of the resolved jet category.

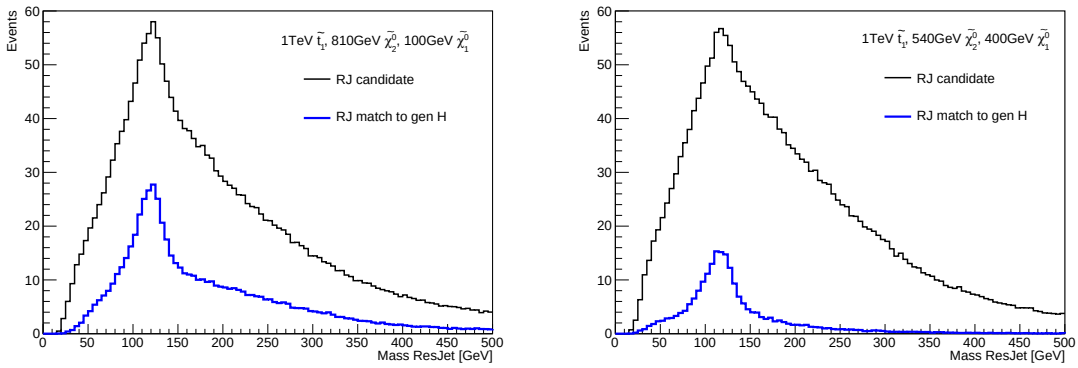

Figure 4.9: Resolved Jet mass distribution for high and low p_T Higgs signal model before applying baseline selections. The black curve shows invariant mass of two b-jets and the blue curve shows invariant mass when the Resolved Jet is matched to generator level Higgs particle.

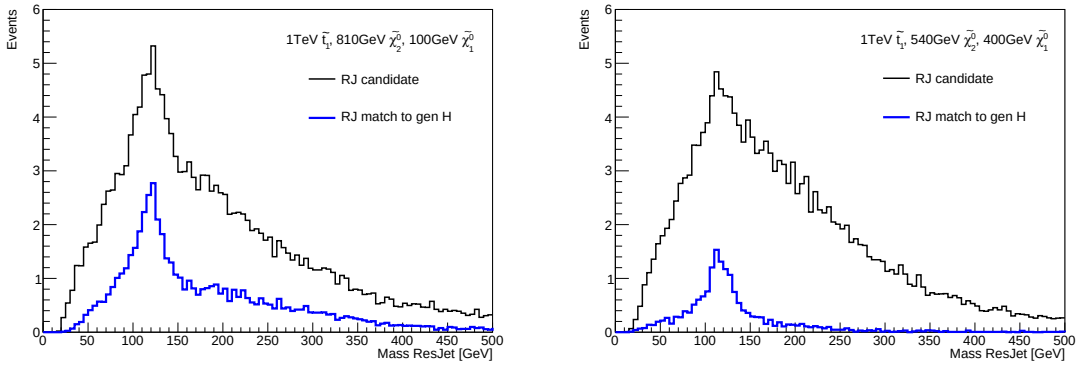

Figure 4.10: Resolved Jet mass distribution for high and low p_T Higgs signal model after applying baseline selections. The black curve shows invariant mass of two b-jets and the blue curve shows invariant mass when the Resolved Jet is matched to generator level Higgs particle.

The following figures (4.11 to 4.15) show the kinematic distributions (MET, M_T, H_T, N_J, and N_{bJ}) and their comparisons after baseline selections (left plots) with additional requirement of Fat Jet (middle plots) or Resolved Jet (right plots). The Fat Jet satisfies $p_T \geq$300 GeV, $|\eta| \leq$2.4, and 100<M_{FJ}<150 GeV. The Resolved Jet satisfies 100<M_{bb}<150 GeV and is selected only for events with zero tagged Fat Jet.

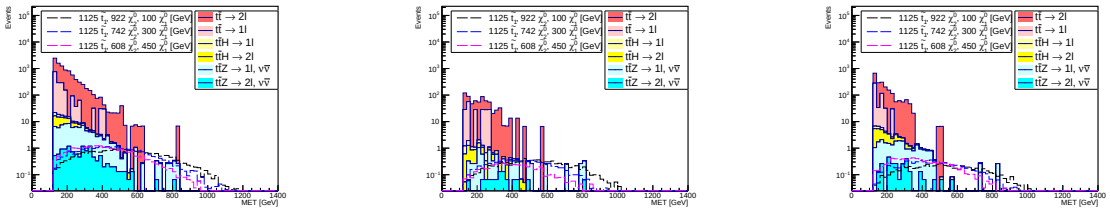

(a) Baseline (b) Baseline + FJ (c) Baseline + FJ=0 + RJ

Figure 4.11: MET after baseline selections and Fat Jet or Resolved Jet requirement

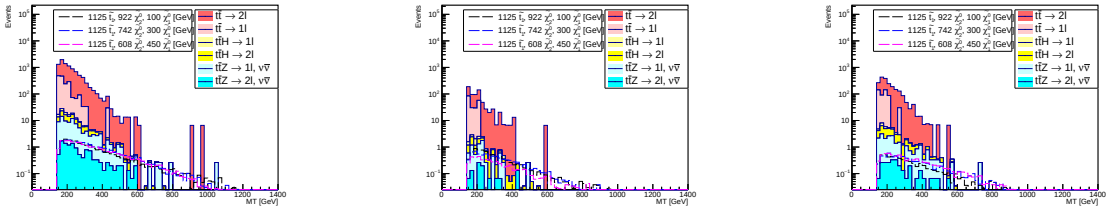

(a) Baseline (b) Baseline + FJ (c) Baseline + FJ=0 + RJ

Figure 4.12: M_T after baseline selections and Fat Jet or Resolved Jet requirement

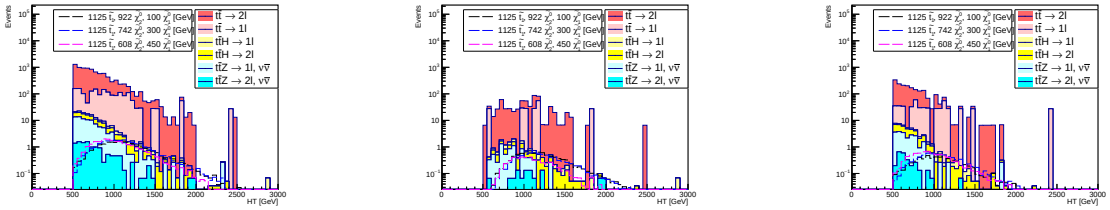

(a) Baseline (b) Baseline + FJ (c) Baseline + FJ=0 + RJ

Figure 4.13: H_T after baseline selections and Fat Jet or Resolved Jet requirement

Table 4.5 and 4.6 shows the number of events survived after applying the various selections on Fat Jets for background and signal process respectively. Table 4.7 shows the significance $\frac{S}{\sqrt{S+B}}$ and $\frac{S}{\sqrt{S+B+0.2B}}$ for the various selections where S is the event yield for signal process, B is for total background yield assuming 20% uncertainty on background yield. The higher the significance value, the better is that particular selection.

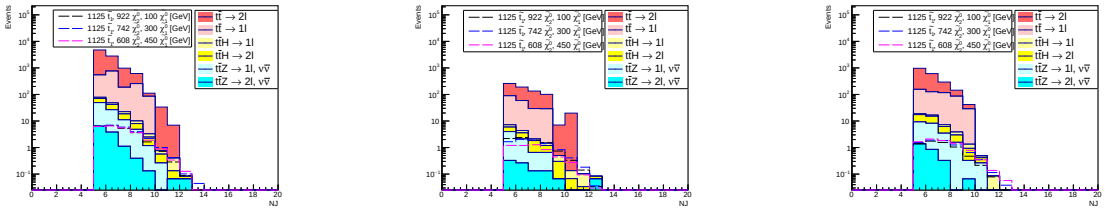

(a) Baseline (b) Baseline + FJ (c) Baseline + FJ=0 + RJ

Figure 4.14: N_J after baseline selections and Fat Jet or Resolved Jet requirement

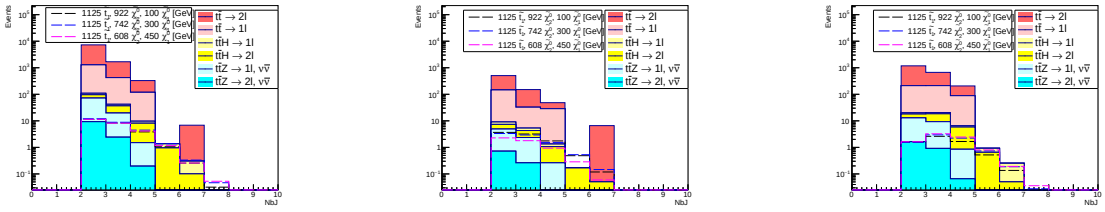

(a) Baseline (b) Baseline + FJ (c) Baseline + FJ=0 + RJ

Figure 4.15: N_{bJ} after baseline selections and Fat Jet or Resolved Jet requirement

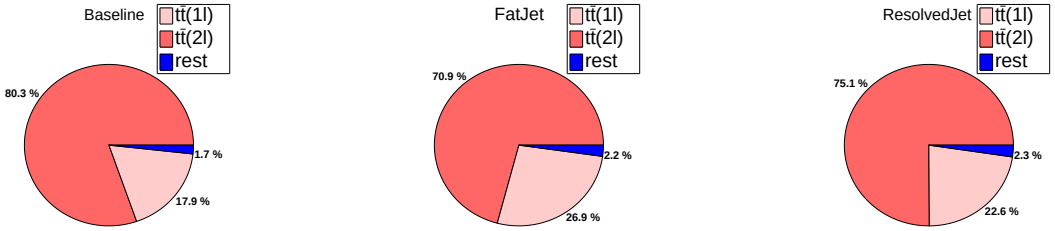

(a) N^{tot}_{evts}=9294.27 (b) N^{tot}_{evts}=711.37 (c) N^{tot}_{evts}=2058.17

Figure 4.16: Background composition after baseline selections and Fat Jet or Resolved Jet requirement.

Selection	$t\bar{t} \to 1\ell$	$t\bar{t} \to 2\ell$	$t\bar{t}H \to 1\ell$	$t\bar{t}H \to 2\ell$	$t\bar{t}Z \to 1\ell$	$t\bar{t}Z \to 2\ell$	Total Bkg
Baseline	1666.95	7465.01	20.55	48.59	81.28	11.89	9294.27
FJ(SD)	300.59	694.11	3.95	7.49	10.19	1.18	1017.51
FJ (SD p_T η)	191.29	504.21	2.94	5.42	6.53	0.98	711.37
FJ (SD p_T η τ_{21})	191.28	491.12	2.74	5.10	6.01	0.98	697.23
RJ (0 FJ)	464.56	1545.39	5.29	19.93	20.39	2.61	2058.17
RJ	573.87	1623.96	6.49	22.72	22.22	2.74	2252

Table 4.5: Event yields for background processes after the selection cuts.

Selection	(1125, 922, 100)	(1125, 512, 100)	(1125, 832, 200)	(1125, 462, 200)
Baseline	24.79	25.41	25.72	27.05
FJ (SD)	10.09	9.98	10.2	10.01
FJ (SD p_T η)	9.24	8.92	9.15	8.81
FJ (SD p_T η τ_{21})	8.47	8.19	8.3	8.01
RJ (0 FJ)	6.52	6.26	6.92	7.38
RJ	11.6	10.64	11.67	11.8

Table 4.6: Event Yield for signal processes where the three numbers indicate masses of sparticles M($\tilde{t_1}$, $\tilde{\chi_2^0}$, $\tilde{\chi_1^0}$).

Selection	(1125, 922, 100)	(1125, 512, 100)	(1125, 832, 200)	(1125, 462, 200)
Baseline	0.26 (0.23)	0.26 (0.24)	0.27 (0.24)	0.28 (0.26)
FJ (SD)	0.31 (0.29)	0.31 (0.28)	0.32 (0.29)	0.31 (0.29)
FJ (SD p_T η)	0.34 (0.31)	0.33 (0.30)	0.34 (0.31)	0.33 (0.30)
FJ (SD p_T η τ_{21})	0.32 (0.29)	0.31 (0.28)	0.31 (0.29)	0.3 (0.28)
RJ (0 FJ)	0.14 (0.13)	0.14 (0.13)	0.15 (0.14)	0.16 (0.15)
RJ	0.24 (0.22)	0.22 (0.20)	0.25 (0.22)	0.25 (0.23)

Table 4.7: Significance $\frac{S}{\sqrt{S+B}}$ and $(\frac{S}{\sqrt{S+B+0.2B}})$ of the corresponding selection cuts for few signal mass points M($\tilde{t_1}$, $\tilde{\chi_2^0}$, $\tilde{\chi_1^0}$), assuming 20% uncertainty on background events. Fat Jet with p_T and $|\eta|$ cuts has the highest significance value, hence the best selection.

Selection	(1125, 922, 100)	(1125, 512, 100)	(1125, 832, 200)	(1125, 462, 200)
Baseline only	2.562	2.199	2.274	2.174
FJ (SD)	0.988	1.101	1.012	1.115
FJ (SD p_T η) [**A**]	1.098	1.37	1.184	1.386
FJ (SD p_T η τ_{21})	1.179	1.458	1.278	1.493
RJ (0 FJ) [**B**]	1.234	1.336	1.219	1.222
Combined (**A**+**B**)	0.757	0.876	0.782	0.842

Table 4.8: Upper limit on r-values for the corresponding selection cuts for few signal mass points. MC statistical and 20% systematic uncertainty is assigned to both signal and background processes while calculating r-value using Combine Tool.

M($\tilde{t_1}$, $\tilde{\chi_2^0}$, $\tilde{\chi_1^0}$) [GeV]	r-value	M($\tilde{t_1}$, $\tilde{\chi_2^0}$, $\tilde{\chi_1^0}$) [GeV]	r-value	M($\tilde{t_1}$, $\tilde{\chi_2^0}$, $\tilde{\chi_1^0}$) [GeV]	r-value
(1000, 810, 100)	0.369	(1125, 922, 100)	0.757	(1150, 607, 475)	1.238
(1000, 720, 200)	0.301	(1125, 932, 200)	0.782	(1165, 958, 100)	1.005
(1000, 630, 300)	0.326	(1125, 742, 300)	0.822	(1165, 868, 200)	0.978
(1000, 5580, 380)	0.405	(1125, 652, 400)	1.005	(1165, 778, 300)	1.063
(1000, 540, 400)	0.537	(1125, 630, 425)	1.013	(1165, 734, 350)	1.104
(1100, 900, 100)	0.649	(1125, 608, 450)	1.109	(1165, 688, 400)	1.199
(1100, 810, 200)	0.655	(1150, 945, 100)	0.871	(1175, 968, 100)	1.031
(1100, 720, 300)	0.734	(1150, 855, 200)	0.876	(1175, 958, 200)	1.016
(1100, 675, 350)	0.792	(1150, 765, 300)	0.954	(1175, 958, 300)	1.083
(1100, 648, 380)	0.869	(1150, 720, 350)	1.006	(1175, 958, 350)	1.184
(1100, 630, 400)	0.868	(1150, 675, 400)	1.101	(1175, 958, 400)	1.253
(1100, 585, 450)	0.984	(1150, 630, 450)	1.258	(1175, 958, 450)	1.370
(1185, 976, 100)	1.081	(1185, 662, 450)	1.454	(1200, 990, 100)	1.244
(1185, 886, 200)	1.071	(1185, 634, 480)	1.443	(1200, 900, 200)	1.270
(1185, 796, 300)	1.150	(1200, 1035, 50)	1.204	(1200, 810, 300)	1.276
(1185, 706, 400)	1.376	(1200, 1008, 80)	1.219	(1200, 720, 500)	1.680

Table 4.9: Upper limit on r-values for the various signal mass point for $x = 0.9$ SUSY mass spectra for the combined search regions with Fat Jets and Resolved Jets.

M($\tilde{t_1}$, $\tilde{\chi_2^0}$, $\tilde{\chi_1^0}$) [GeV]	r-value	M($\tilde{t_1}$, $\tilde{\chi_2^0}$, $\tilde{\chi_1^0}$) [GeV]	r-value	M($\tilde{t_1}$, $\tilde{\chi_2^0}$, $\tilde{\chi_1^0}$) [GeV]	r-value
(1000, 450, 100)	0.408	(1125, 512, 100)	0.876	(1150, 525, 100)	1.021
(1000, 400, 200)	0.460	(1125, 462, 200)	0.842	(1150, 475, 200)	1.176
(1000, 390, 220)	0.503	(1125, 438, 250)	1.032	(1150, 450, 250)	1.233
(1000, 378, 245)	0.494	(1125, 422, 280)	1.030	(1150, 435, 280)	1.253
(1100, 500, 100)	0.780	(1140, 520, 100)	0.972	(1175, 538, 100)	1.179
(1100, 450, 200)	0.836	(1140, 470, 200)	1.047	(1175, 488, 200)	1.282
(1100, 425, 250)	0.910	(1140, 445, 250)	1.132	(1175, 462, 250)	1.284
(1100, 410, 280)	0.872	(1140, 430, 280)	1.147	(1175, 448, 280)	1.399

Table 4.10: Upper limit on r-values for the various signal mass point for $x = 0.5$ SUSY mass spectra for the combined search regions with Fat Jets and Resolved Jets.

M($\tilde{t_1}$, $\tilde{\chi_2^0}$, $\tilde{\chi_1^0}$) [GeV]	r-value	M($\tilde{t_1}$, $\tilde{\chi_2^0}$, $\tilde{\chi_1^0}$) [GeV]	r-value	M($\tilde{t_1}$, $\tilde{\chi_2^0}$, $\tilde{\chi_1^0}$) [GeV]	r-value
(1000, 190, 50)	0.579	(1075, 200, 75)	1.027	(1100, 205, 75)	1.098
(1025, 195, 50)	0.675	(1085, 207, 50)	1.001	(1125, 215, 50)	1.304
(1050, 200, 50)	0.805	(1085, 202, 75)	1.059	(1150, 220, 50)	1.424
(1075, 205, 50)	0.939	(1100, 210, 50)	1.158	(1200, 222, 90)	2.044

Table 4.11: Upper limit on r-values for the various signal mass point for $x = 0.2$ SUSY mass spectra for the combined search regions with Fat Jets and Resolved Jets.

The CMS collaboration has developed a software called Higgs Combine Tool [41, 42, 43, 44] which is used for calculating the upper limits on the signal points. This is a cut and count analysis where the expected number of signal and background events, number of events observed in data and the associated systematic uncertainties is provided. In this thesis the study of data is out of scope and hence the observed number of events is set equal to the total number of background events.

The p-value is the significance of a deviation in data of the observed event yield from the predicted yield under a given hypothesis. For exclusion of a signal model, we look at the deviation of the observed yield from the signal+background predicted yield. This is done in every search region.

The expected event yield is given as

$$n_i^{exp} = \mu s_i + b_i \tag{4.5}$$

where μ is the signal strength, varying from 0 to 1, and s_i and b_i are the number of events of signal and background process respectively in bin i. If $\mu = 0$, signal is absent which corresponds to the background-only (null) hypothesis and if $\mu = 1$, the signal is present exactly as predicted by the theory at the given cross-section.

Likelihood function is defined as the probability of the observed data given the model parameters. In simpler words, the likelihood function quantifies the agreement between the observed data and the prediction for a given hypothesis (parameter μ in our case). A variable called the test statistic (sometimes called likelihood ratio) is used to distinguish between background only and signal+background hypothesis. It is defined using likelihood function for the two hypotheses.

The exclusion potential for a given signal model can be found from the upper limits on the value of parameter r (same as μ) which is calculated with 95% confidence level where r is defined as

$$r = \frac{Number\ of\ observed\ signal\ events}{Number\ of\ expected\ signal\ events} \tag{4.6}$$

The number of events is integrated luminosity ($\mathscr{L}$) multiplied by signal cross-section (σ), which is $N_{evt} = \mathscr{L} * \sigma$ assuming unit acceptance and efficiency. Thus the parameter r can be written as,

$$r = \frac{\sigma_{observed}}{\sigma_{expected}} \tag{4.7}$$

where $\sigma_{observed}$ is the observed cross-section of the signal process (assuming null hypothesis) and $\sigma_{expected}$ is the theoretically calculated cross-section from the model (assuming signal+background hypothesis). Thus, a limit on r gives a limit on signal cross-section. If the limit on r is found to be less than 1, it means that the observed cross-section is small than theoretically expected, which implies that the signal model is excluded.

Datacards are created for each search bin and the input to these datacards are the signal and background yields in the different search bins. We have assigned MC statistical uncertainty and 20% systematic uncertainty for single lepton analysis and 50% systematic uncertainty for fully hadronic analysis. This is done for both signal and background processes in both analyses. The Higgs Combine Tool then computes the upper limit on value of r at 95% confidence level (CL).

4.3 Results for single lepton analysis

Exclusion limits with 95% Confidence Level (CL) are calculated for the three mass spectra scenarios shown in figure 4.17 assuming 20% systematics and 150 fb^{-1} luminosity. The three scenarios are defined by the mass spectra relation where $M(\tilde{\chi}_2^0) = x\ \Delta M(\tilde{t}_1, \tilde{\chi}_1^0)$. The single lepton analysis excludes stop mass until 1185 GeV for $x = 0.9$, until 1150 GeV for $x = 0.5$ and uptil 1100 GeV for $x = 0.2$.

The limits improve significantly on adding a Higgs requirement as compared to only baseline selections. Table 4.8 shows the enhancement in r-values from first row with baseline selections to last row with additional Higgs requirement (Fat Jet and Resolved Jet combined).

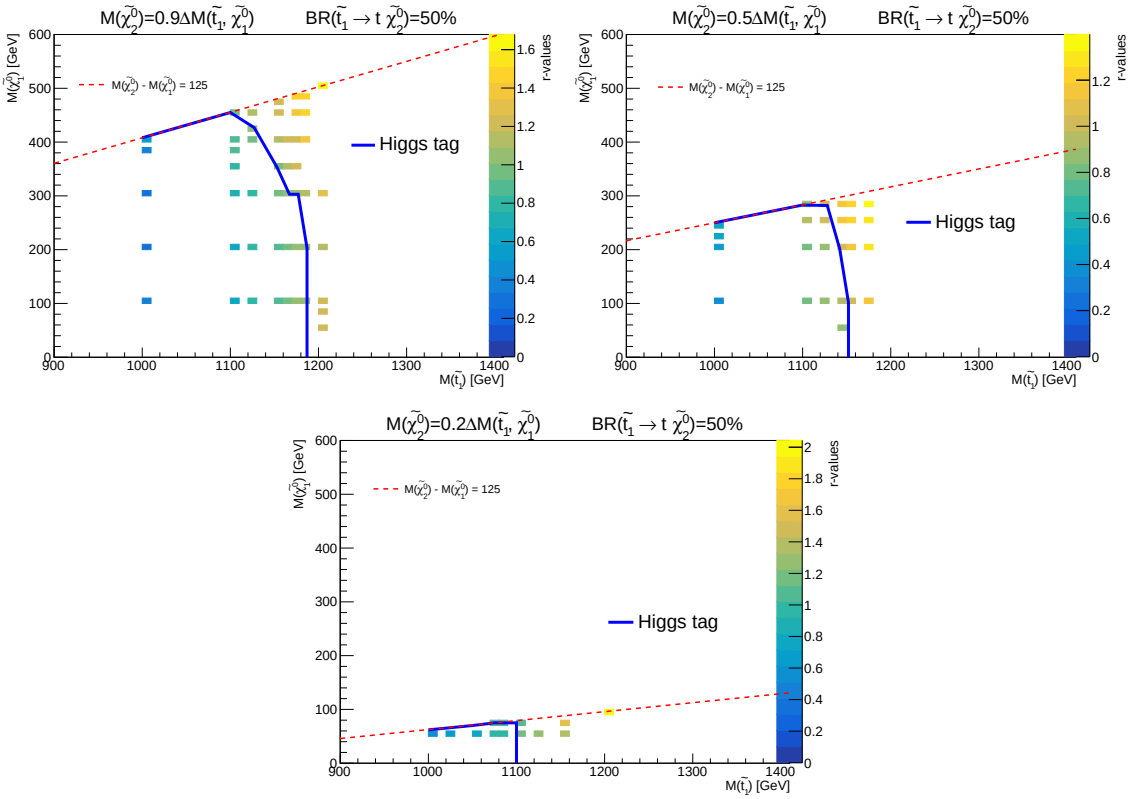

Figure 4.17: Expected limits at 95% confidence level for stop pair production with 50% - 50% branching ratio to $\tilde{\chi}_2^0$ - $\tilde{\chi}_1^0$. The region above the red dotted line is kinematically not allowed for on-mass shell particles. The solid blue line shows limit curve using baseline selections and Higgs tagging. The three plots are for mass fraction 0.9, 0.5 and 0.2.

.

Chapter 5

Stop search in fully hadronic channel using Higgs tagging

For $t\bar{t}$ process where both tops decay hadronically, the branching ratio is around 46% which being the dominant decay mode makes it an important channel to study. Dedicated searches are designed by the CMS collaboration to search for stop pairs in fully hadronic final state with jets plus MET as signature. This thesis involves the study of such an analysis. We check the sensitivity of this analysis to our signal model without and with using Higgs tagging. The SUSY signal process has hadronically decaying top quarks, and Higgs boson which will give large number of jets in the final state. There is also significant missing transverse momentum due to the LSPs in the event, hence the classic signature of jets plus MET. The SM processes which gives jets and MET in the final state are the dominant backgrounds for this search. There are multijet (QCD), W+jets, Z+jets and $t\bar{t}$ process. There can be contribution from other processes like WW, ZZ, WZ, etc but these are small, hence we ignore them.

In this analysis, the simulated samples of signal process is generated using MadGraph, Pythia and Delphes. However, for the background processes, they are centrally generated using CMS event generation machinery called CMSSW in the following. Before using the samples generated from these two methods, we first need to make sure that they are compatible and can be used to compare signal and backgrounds in a meaningful way.

CMSSW is a Geant4 [45] based detector simulation which uses full-simulation where the response of the CMS detector to the various particles is modelled in detail. This gives

realistic detector effects on the measured events. The background samples are generated using the full-sim and these samples were centrally generated and were provided to me by Dr Aditee Rane, a PhD student in our EHEP lab.

The Delphes uses fast-simulation information to model the detector response to the particles from collision event. The advantage of using fast-simulation is its speed which is two to three orders of magnitude larger than the full-simulation. In our analysis, the SUSY model parameters are unknown and hence we need to scan the parameter space and generate signal samples for various possible parameter values which in our case are the sparticle masses. This requires us to generate huge amounts of sample and hence fast-simulation is the better option here. Due to time constraints of this thesis project, we generated the signal samples using Delphes instead of CMSSW fast-simulation.

The Delphes and CMSSW reconstruction level objects are studied and they are found to match to a good extent. The process studied is $pp \rightarrow \tilde{t_1}\tilde{t_1^*}$ and $\tilde{t_1} \rightarrow t\tilde{\chi_1^0}$ where M($\tilde{t_1}$) = 700 GeV and M($\tilde{\chi_1^0}$) = 500 GeV. One sample is generated using Delphes simulation and other is taken from centrally generated CMSSW which used fast simulation. Fig. 5.1 shows the p_T of gen level leptons (e and μ) matched with the reco level leptons in ΔR of 0.2. The p_T distributions from Delphes and CMS seems to match reasonably for the purpose of this thesis. MET at reconstruction level is also found to match reasonably for the two samples.

There exist several analyses with Jets+MET final state signature [15, 16, 46]. The goal of this section is to first study the fully hadronic analysis and add Higgs requirement in addition to the analysis [47] and check for any improvement in the exclusion potential of this search.

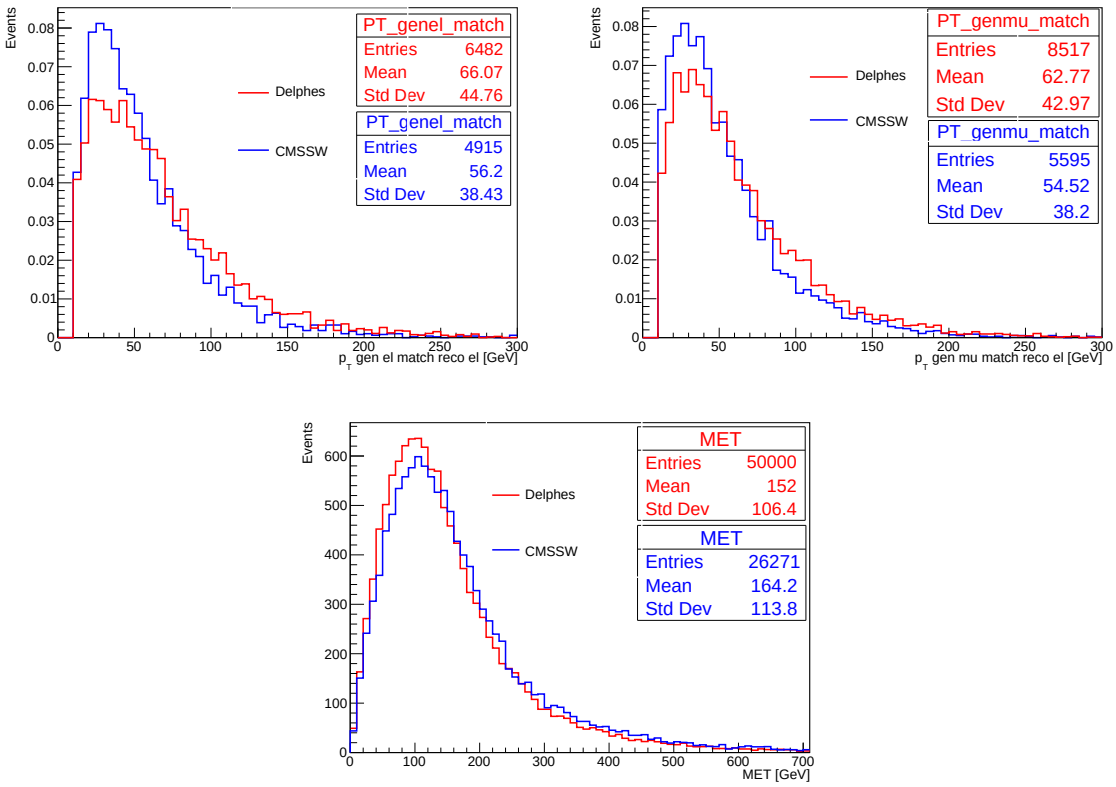

Figure 5.1: p_T distribution of gen level e (left plot) and μ (right plot) and reconstructed MET distribution (bottom plot) comparing Delphes (red) and CMSSW (blue) simulation.

Background sources

For the fully hadronic final state, the major backgrounds considered are:

- QCD jets: The cross section of QCD process is orders of magnitude higher than the stop signal process at LHC. MET in these events arises from energy mismeasurements of jets. Even if this fraction is small, due to its extremely high cross section, there can be significant number of such events in the signal region.

- W+jets: If the W boson decays leptonically but the lepton fails selection, the event can give jets + MET signature. The W can also decay to a tau lepton which then decays hadronically. These events can also pass the event selection and enter the signal regions.

- Z+jets: In events where the Z boson decays to neutrino-antineutrino pair is a potential source of background where the νs will contribute to event MET. Another possibility is when the Z decays leptonically but both the leptons fails the event selections and give jets + MET signature. However, the fraction where both the leptons fail is very low and hence we ignore these events.

- $t\bar{t}$: The top quark decays to b-quark and W boson. These events have similar reasons as W+jets process where the lost lepton from W and/or hadronically decaying tau from W can pass event selections and contribute to jets + MET signature.

5.1 Event selection

Selection cuts are applied on events to reduce the SM background events and retain signal events. The event selections are slightly different for the Delphes and CMSSW generated samples. Some additional event cleaning filters are applied on the background samples to reject spuriously high MET events.

For background samples

- Event cleaning filters: globalSuperTightHalo2016Filter, HBHENoiseFilter, HBHEIsoNoiseFilter, EcalDeadCellTriggerPrimitiveFilter, ecalBadCalibReducedFilter, eeBadScFilter, BadChargedCandidateFilter, BadPFMuonFilter

- $H_T^{miss}/H_T < 1$

- PFCaloMETRatio < 5

- Veto event if a jet has $p_T > 200$ GeV, muonEnergyFraction > 0.5 and $\Delta\phi(J, MET) > \pi$ - 0.4

- Veto event if leading jet has neutralEmEnergyFraction¡0.03 and $\Delta\phi(J1, MHT) > \pi$ - 0.4

- Veto electron with $p_T \geq 20$ GeV and $|\eta| \leq 2.5$

- Muon veto with $p_T \geq 20$ GeV and $|\eta| \leq 2.4$

- Veto isolated tracks
- Atleast 4 AK4 jets with $p_T \geq 30$ GeV and $|\eta| \leq 2.4$
- Atleast 2 b-tagged AK4 jets with $p_T \geq 30$ GeV and $|\eta| \leq 2.4$. To tag a jet as b-jet, the variable bDiscriminatorCSV > 0.8 is used.
- $H_T \geq 600$ GeV
- MET$\geq$ 200 GeV
- $\Delta\phi(J_{1,2}, MET) \geq 0.5$ and $\Delta\phi(J_{3,4}, MET) \geq 0.3$ where $J_{1,2,3,4}$ are jets in decreasing order of p_T

For signal samples

- Electron veto with $p_T \geq 20$ GeV and $|\eta| \leq 2.5$
- Muon veto with $p_T \geq 20$ GeV and $|\eta| \leq 2.4$
- Atleast 4 AK4 jets with $p_T \geq 30$ GeV and $|\eta| \leq 2.4$
- Atleast 2 b-tagged AK4 jets with $p_T \geq 30$ GeV and $|\eta| \leq 2.4$. In Delphes b-tagging is done using dR matching to gen level b-quarks
- $H_T \geq 600$ GeV
- MET$\geq$ 200 GeV
- $\Delta\phi(J_{1,2}, MET) \geq 0.5$ and $\Delta\phi(J_{3,4}, MET) \geq 0.3$ where $J_{1,2,3,4}$ are jets in decreasing order of p_T

Figure 5.2 and 5.3 shows the MET and H_T distribution before and after applying baseline selections. These selections helps reduce the backgrounds significantly. There are some unphysical peaks at high values of MET and H_T, especially in the QCD events. These can arise from events having a low gen level H_T but high reco level H_T. Such an event will get a large weight while adding H_T binned samples. Thus, such an event will appear like an abrupt peak in high reco H_T region. The event filters take care of such events. The QCD events are drastically reduced with MET and $\Delta\phi$ cuts along with event cleaning filters. Observe

that most peaks are gone after baseline selection. The signal is not significantly affected by these selections.

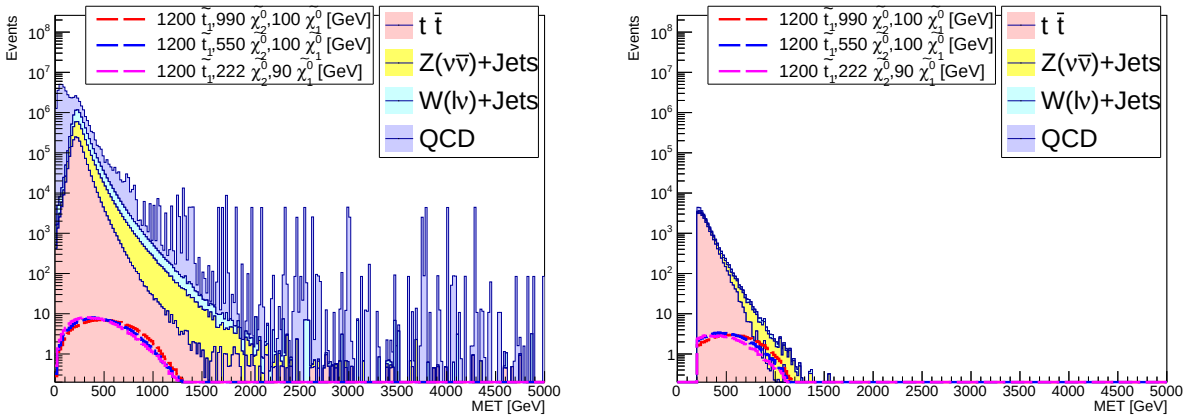

Figure 5.2: MET distribution before (left) and after applying baseline selections (right)

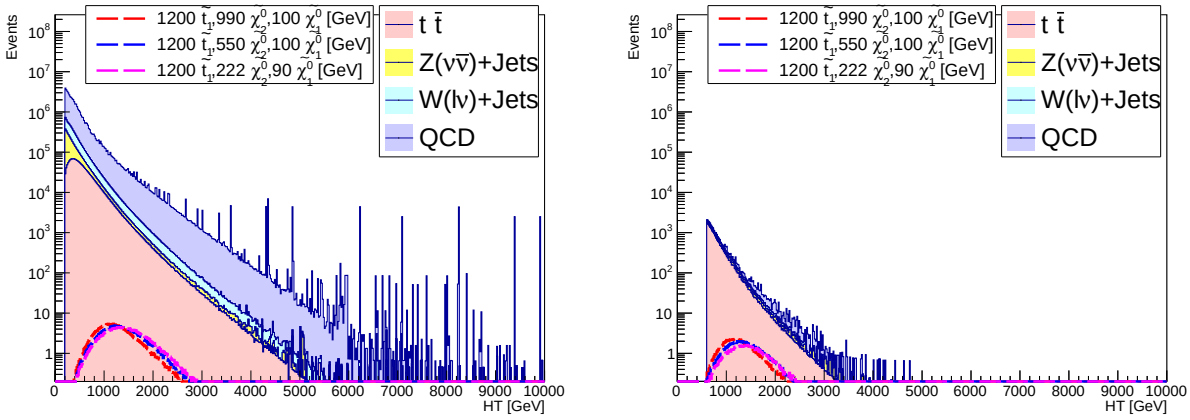

Figure 5.3: H_T distribution before (left) and after applying baseline selections (right)

Figure 5.4 shows the distribution of kinematic variables after applying the baseline selections. Table 5.1 shows the cutflow of sequential event selections for the 4 backgrounds considered and three signal model points with M($\tilde{t_1}$)=1.2 TeV and M($\tilde{\chi_1^0}$)=100 GeV while varying M($\tilde{\chi_1^0}$) for three scenarios with x=0.9, 0.5, and 0.2. Table 5.2 shows the number of events (in percentage) that pass the sequentially applied event selections with respect to no selection. Observe the significant reduction in all backgrounds with MET$\geq$ 200 GeV cut. However, the signal process does not have such a drastic reduction with MET cut implying that high MET is a good selection.

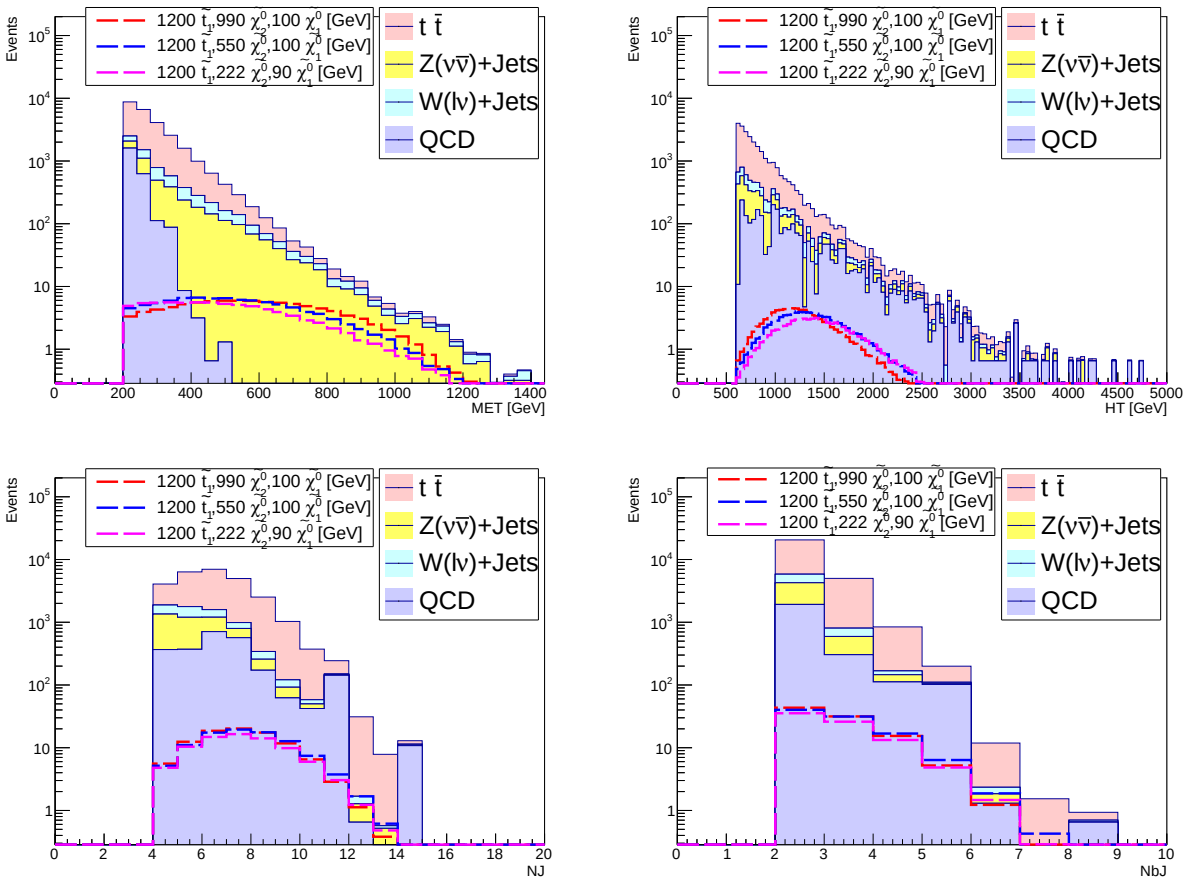

Figure 5.4: Kinematic distributions after applying baseline selections.

Selection	$t\bar{t}$	W+Jets	$Z(\nu\bar{\nu})$+Jets	QCD	Total Bkg	x=0.9	x=0.5	x=0.2
No cut	1699753	3986378	2513252	37738195	45937577	255	255	255
N_ℓ=0	809976	2589842	2464534	29333500	35197852	199	200	201
MET$\geq$ 200 GeV	113342	472284	600304	415533	1601462	180	177	171
$N_J \geq 4$	88344	112213	92741	198473	491772	172	170	164
$N_{bJ} \geq 2$	43278	5103	4575	14498	67453	119	123	117
$H_T \geq$ 600 GeV	43020	5065	4522	14498	67105	118	122	116
$\Delta\phi(J_{12}, \vec{p}_T^{miss})\geq$0.5 $\Delta\phi(J_{34}, \vec{p}_T^{miss})\geq$0.3	22345	2620	3475	290	28731	97	97	81
Isotrackveto and Filters	11726	1544	3233	126	16628	97	97	81

Table 5.1: Cutflow table for sequentially applied baseline selections.

Selection	$t\bar{t}$	W+Jets	$Z(\nu\bar{\nu})$+Jets	QCD	Total Bkg	x=0.9	x=0.5	x=0.2
No cut	100	100	100	100	100	100	100	100
N_ℓ=0	48	65	98	78	77	78	79	79
MET$\geq$ 200 GeV	6.7	12	24	1.1	3.5	71	69	67
$N_J \geq 4$	5.2	2.8	3.7	0.52	1.1	68	66	64
$N_{bJ} \geq 2$	2.5	0.13	0.18	0.04	0.15	47	48	46
$H_T \geq 600$ GeV	2.5	0.13	0.18	0.04	0.15	46	48	46
$\Delta\phi(J_{12}, \vec{p}_T^{miss})\geq 0.5$ $\Delta\phi(J_{34}, \vec{p}_T^{miss})\geq 0.3$	1.3	0.06	0.14	0.0007	0.06	38	38	32
Isotrackveto and Filters	0.69	0.04	0.13	0.0003	0.04	38	38	32

Table 5.2: Cutflow table for sequentially applied baseline selections. The table shows percentage of events survived with respect to no selection.

Contribution from individual backgrounds can be studied from the pie charts in figure 5.5. QCD events are drastically reduced by MET and $\Delta\phi$ cuts. The major background after baseline selections is from $t\bar{t}$ process.

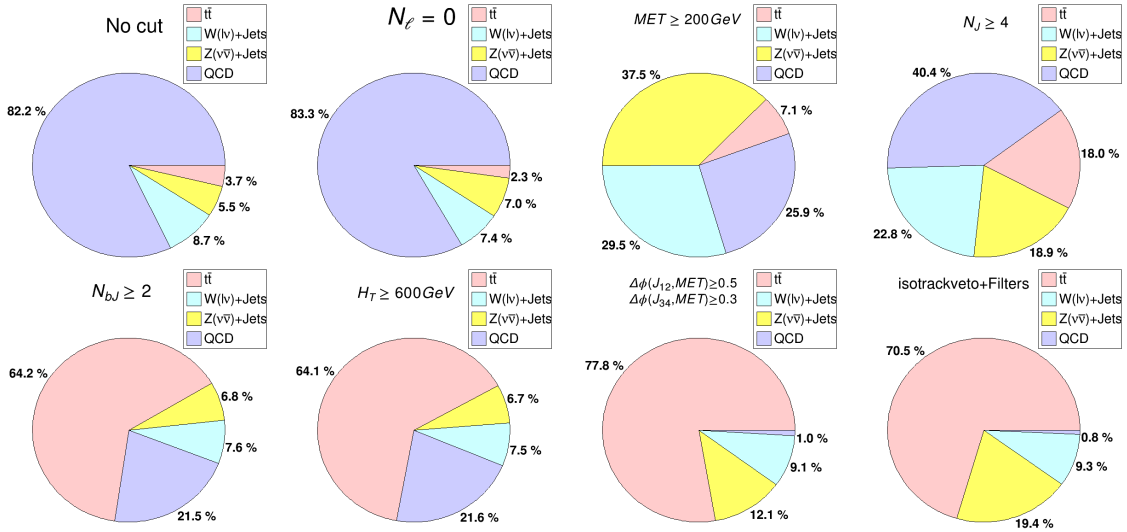

Figure 5.5: Pie chart showing background composition with sequential baseline selections.

Higgs tagging

The strategy to reconstruct the Higgs particle in the event is same as used in the single lepton analysis. Two categories are studied. Fat Jets are used to target high p_T Higgs whose decay products are collimated and lie within an AK8 jet. To improve the tagging, a p_T cut of 300 GeV and $|\eta|$ cut of 2.4 is applied on these Fat Jets. Along with this, $\tau_{21} \leq 0.6$ and $100 < M_{FJ} < 150$ GeV is also applied. For scenarios where the Higgs does not have considerable boost to form an AK8 jet, a resolved jet category is used. The invariant mass of two b-jets falling in Higgs window is called as Higgs Resolved Jet. Events with zero Fat Jet and atleast one Resolved Jet are selected in the second category. Figure 5.6 shows the MET distribution of events with baseline selection applied and of events falling in the two categories as mentioned above.

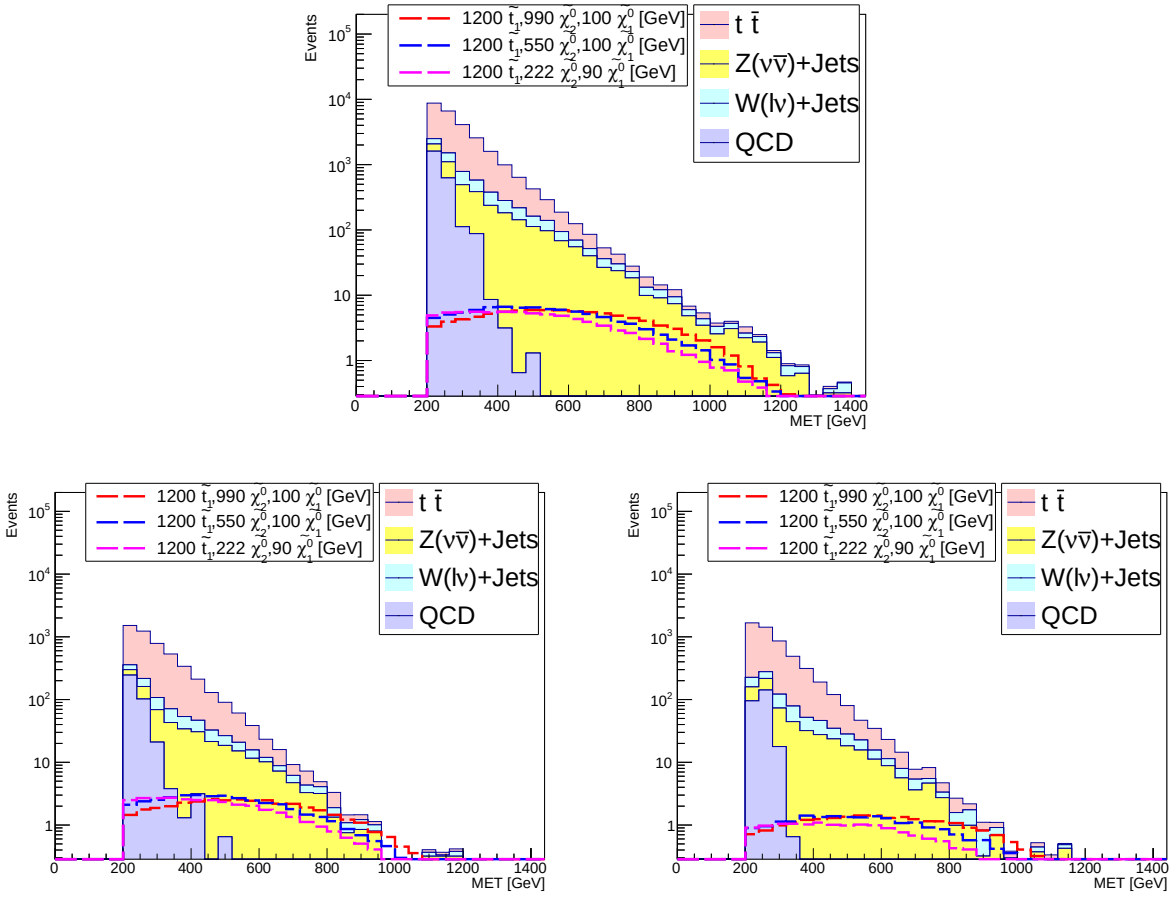

Figure 5.6: MET distribution after baseline selections (top), with Fat Jet requirement (left bottom) and with ResolvedJet requirement in absence of Fat Jet (right bottom).

Selection	$t\bar{t}$	W+Jets	$Z(\nu\bar{\nu})$+Jets	QCD	Total bkg	x=0.9	x=0.5	x=0.2
Baseline	11725.5	1544.2	3232.8	125.6	16628.1	97.1	97.2	81.4
FJ	3193.5	346.4	694.1	22.0	4256.0	46.7	49.2	41.8
FJ (SD)	2664.8	214.7	439.7	12.1	3331.3	45.9	46.9	40.2
FJ (SD+$p_T\eta$)	2458.9	199.1	400.0	12.1	3070.1	43.3	44.0	37.7
FJ (SD+$p_T\eta$+τ_{21})	2280.3	173.8	338.3	10.8	2803.2	39.0	40.7	35.0
RJ	3501.5	353.9	668.7	4.2	4528.3	43.5	40.5	32.3
RJ (FJ0)	2917.2	301.1	569.3	2.9	3790.5	23.2	21.2	15.9

Table 5.3: Event yields for background and signal processes after the selection cuts.

Multibinning strategy

This analysis is an inclusive search which is designed to have sensitivity to a large number of possibilities of signal model scenarios in contrast with the single lepton analysis which is designed to target specific signal model scenarios. Both kinds of analyses are important. Inclusive searches can get a hint of discovery and targeted searches can pinpoint the discovery to a specific signal model.

Multibin analysis is a classic strategy to search for SUSY at CMS. It is a powerful technique where the multiple search bins have sensitivity to different scenarios of SUSY and the combination of these bins enhances the sensitivity, in contrast with using individual bins. This analysis uses 4-dimensional binning in the variables MET, H_T, N_J and N_{bJ} giving a total of 80 search regions. The N_J and N_{bJ} are binned as: N_J: [4-5], [6-7], [8-9], [$\geq$10] and N_{bJ}: [2], [$\geq$3]. Table 5.4 shows the binning in MET and H_T.

[47] is an inclusive SUSY search which targets a wide range of model scenarios. This analysis uses multibinning strategy and is sensitive to a vast number of SUSY models. The original published analysis used total of 174 search bins, however we are using a subset of only 80 bins with two or more b-tagged jets since these regions are expected to have sensitivity to our signal model of stop pair production.

Bin	MET [GeV]	H_T [GeV]	Bin	MET [GeV]	H_T [GeV]
1	200 - 350	600 - 900	6	350 - 600	>1200
2	200 - 350	900 - 1200	7	600 - 850	600 - 1200
3	200 - 350	>1200	8	600 - 850	>1200
4	350 - 600	600 - 900	9	>850	850 - 1700
5	350 - 600	900 - 1200	10	>850	>1700

Table 5.4: Binning in variable MET and H_T

Figure 5.7 shows the MET distribution after baseline selection (top plot), and additionally requring Fat Jet (bottom left) or Resolved Jet (bottom right) where on requiring FJ or RJ, the contribution from $Z(\nu\bar{\nu})$+Jets process, which is an irreducible background is reduced.

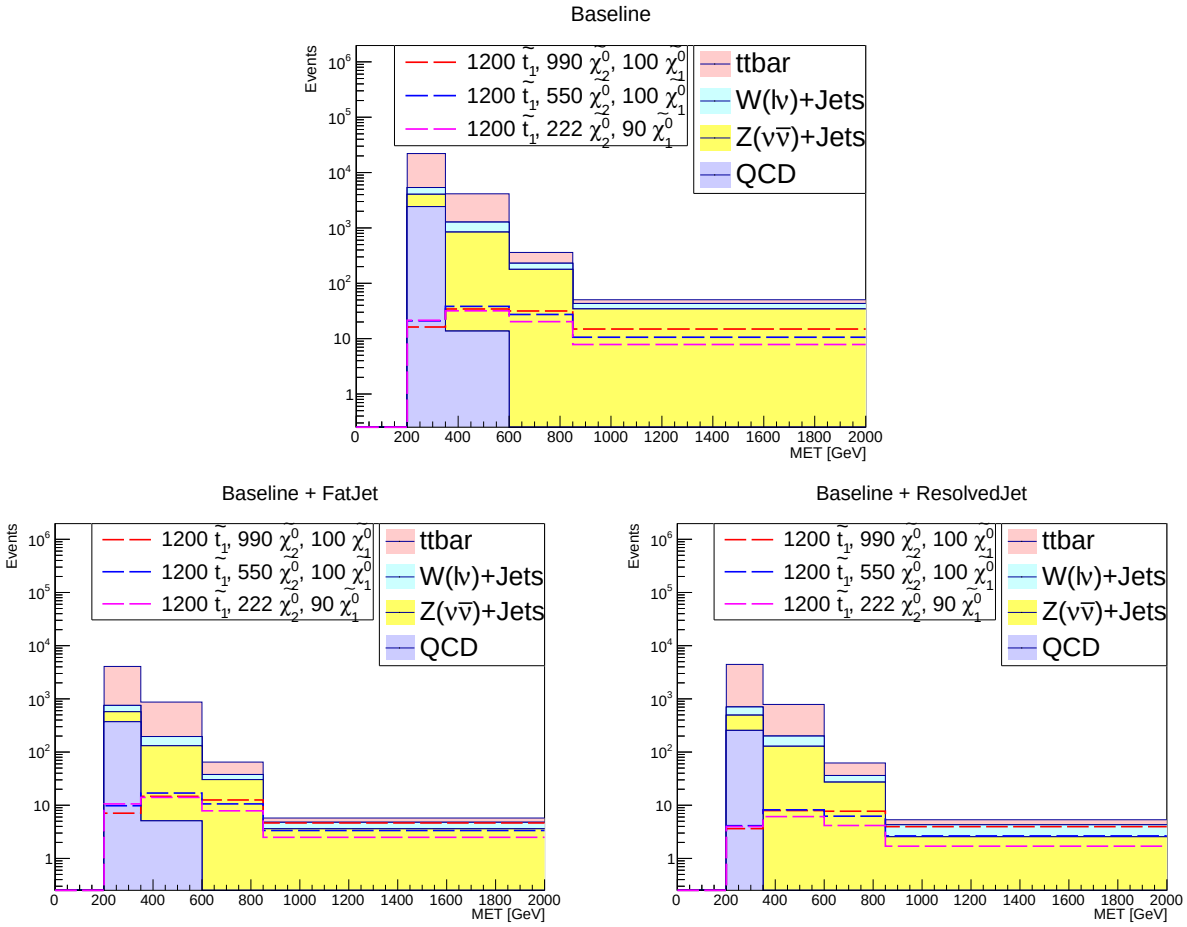

Figure 5.7: MET distribution after baseline, with Fat Jet or Resolved Jet requirement in MET search bins and inclusive in other search variables.

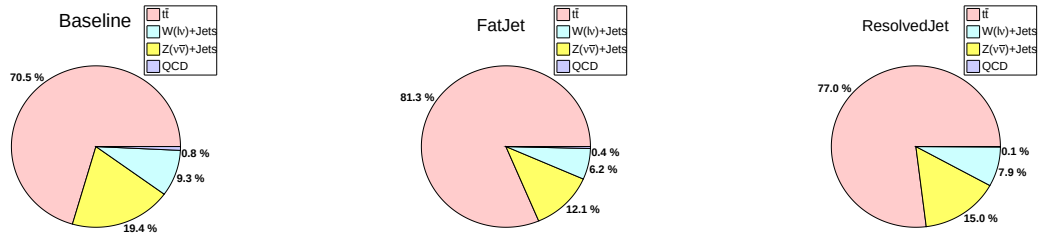

(a) N^{tot}_{evts}=16628.1 (b) N^{tot}_{evts}=2803.2 (c) N^{tot}_{evts}=3790.5

Figure 5.8: Background composition after baseline selections and Fat Jet or Resolved Jet requirement.

5.2 Results for fully hadronic analysis

Exclusion limits with 95% confidence level are calculated for SUSY pair production of stop particles with Higgs boson in its cascade decay. The Higgs is reconstructed in two categories, tagged and resolved. The sensitivity of the fully hadronic analysis with and without Higgs information is studied. Three mass spectra (x = 0.9, 0.5, and 0.2) are considered with 50-50% branching ratio of stop particle to lightest and next lightest neutralino via top quark. MC statistical and 50% systematic uncertainty is assigned to both signal and background processes and the events are scaled to their cross-section and luminosity of 150 fb^{-1} is used.

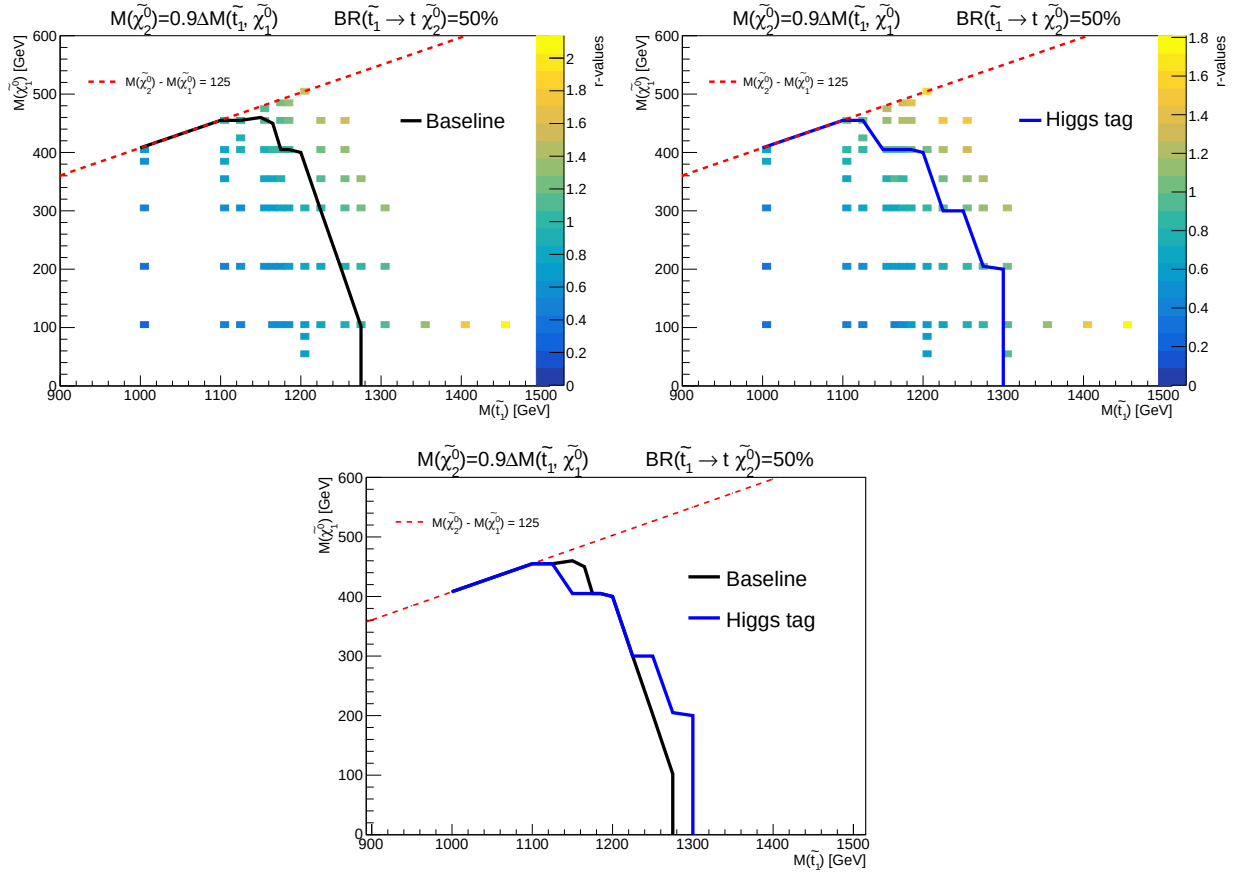

Figure 5.9: Expected limits at 95% confidence level for stop pair production with 50% - 50% branching ratio to $\tilde{\chi}_2^0$ - $\tilde{\chi}_1^0$ and 0.9 mass fraction. The region above the red dotted line is kinematically not allowed for on-mass shell particles. The solid black line shows limit curve using baseline selections only and the solid blue line shows using Higgs tagging in addition to baseline selections. MC statistical and 50 % systematic uncertainty is assigned.

It is found that the inclusive analysis with only baseline selections has good sensitivity to most signal models and on adding Higgs information the sensitivity to stop mass is enhanced by a few tens of GeV. This analysis has good sensitivity to boosted Higgs models but low sensitivity to compressed model scenarios. The 0L analysis excludes stop mass uptil 1.3 TeV for x=0.9, uptil 1.25 TeV for x=0.5, and uptil 1.2 TeV for x=0.2 scenario with baseline selection and Higgs requirement.

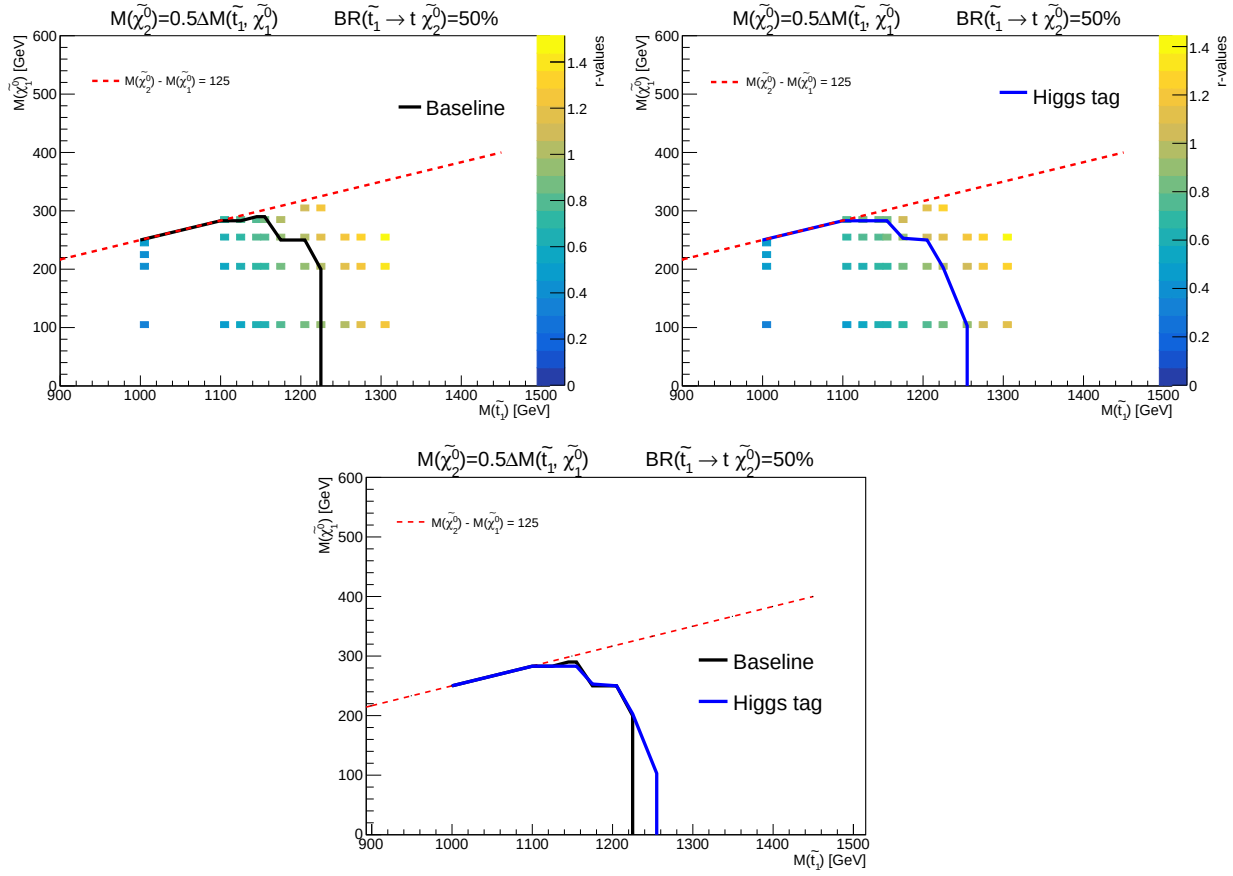

Figure 5.10: Expected limits at 95% confidence level for stop pair production with 50% - 50% branching ratio to $\tilde{\chi}_2^0$ - $\tilde{\chi}_1^0$ and 0.5 mass fraction. The region above the red dotted line is kinematically not allowed for on-mass shell particles. The solid black line shows limit curve using baseline selections only and the solid blue line shows using Higgs tagging in addition to baseline selections. MC statistical and 50 % systematic uncertainty is assigned.

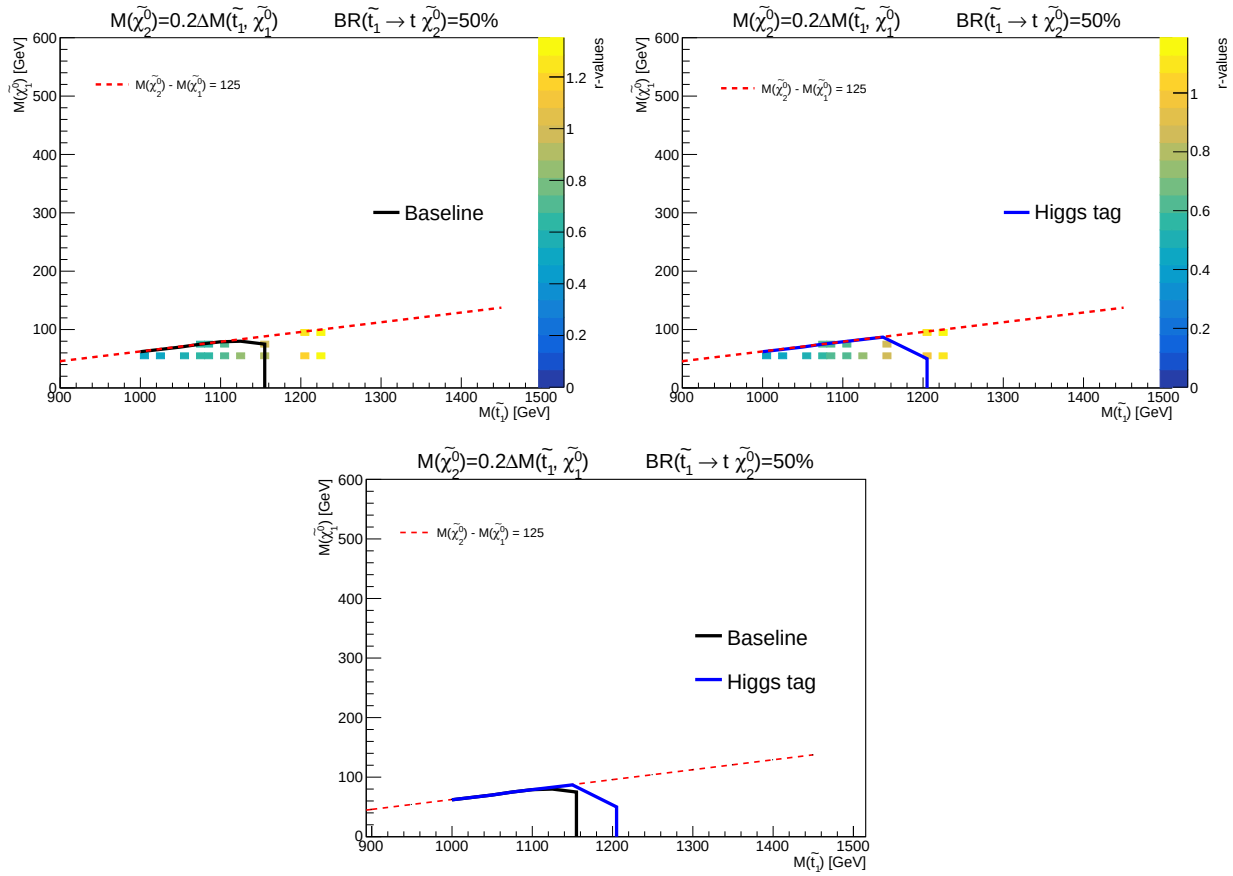

Figure 5.11: Expected limits at 95% confidence level for stop pair production with 50% - 50% branching ratio to $\tilde{\chi}_2^0$ - $\tilde{\chi}_1^0$ and 0.2 mass fraction. The region above the red dotted line is kinematically not allowed for on-mass shell particles. The solid black line shows limit curve using baseline selections only and the solid blue line shows using Higgs tagging in addition to baseline selections. MC statistical and 50 % systematic uncertainty is assigned.

Sensitivity studies by varying branching ratio

The decay probability of the stop particle is a free parameter in the model and we had assumed a 50 - 50 % probability to decay via $\tilde{\chi}_1^0$ and $\tilde{\chi}_2^0$ in our study so far. Now we vary this branching ratio (BR) and study the upper limit on r for a model with fixed masses of SUSY particles. Figure 5.12 shows the upper limit on r-values by varying BR of stop to decay via $\tilde{\chi}_2^0$. The model points below r=1 are excluded by the analysis and the above ones are not sensitive to the analysis. Since the analysis reconstructs the Higgs, acceptance of events with higher BR is higher and hence the sensitivity to models with higher BR is higher. This has the potential to shed light on the nature of the neutralinos, on using data from pp collision events or the available public results.

Being an inclusive analysis, it has sensitivity to a large range of BR even without Higgs tagging for moderate and high p_T Higgs models (top plots in fig. 5.12). The analysis is not sensitive to compressed model scenarios (bottom plot in fig. 5.12).

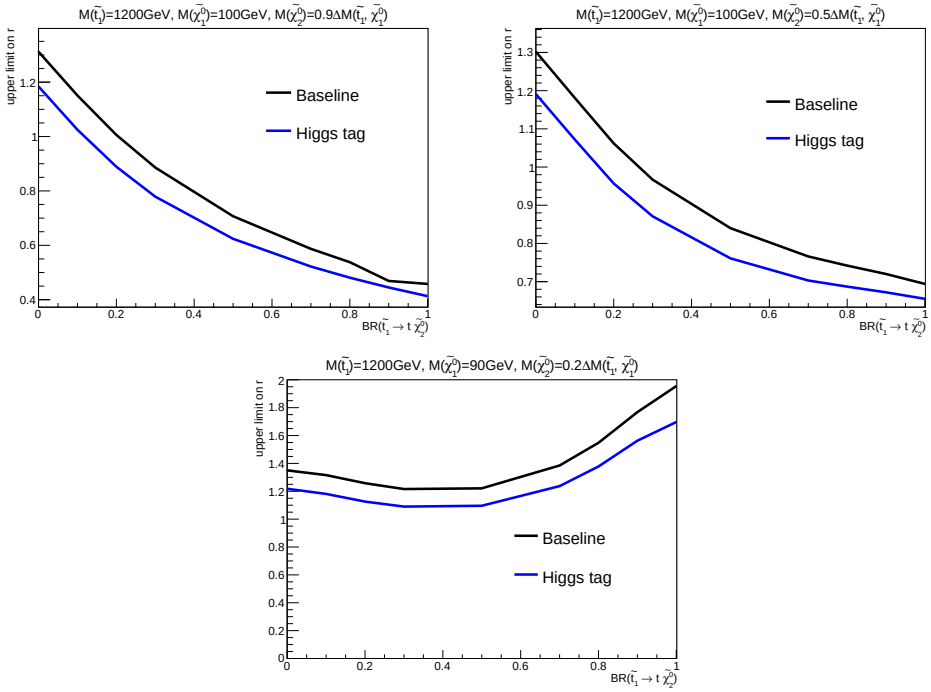

Figure 5.12: Upper limit on r-value at 95% confidence level with varying branching ratio for $\tilde{t_1} \rightarrow t\tilde{\chi}_2^0$ decay for signal model with fixed sparticle masses at M($\tilde{t_1}$)=1.2 TeV, M($\tilde{\chi}_2^0$)=990 GeV, M($\tilde{\chi}_1^0$)=100 GeV.

Chapter 6

Results

The sensitivity of the single lepton (1L) analysis and fully hadronic (0L) analysis is studied and compared. The background and signal events are scaled to their cross-section and a luminosity of 150 fb^{-1} is used. Higgs Combine Tool is used to calculate the upper limits on r-value using the asymptotic method. MC statistical uncertainty is used. 20% and 50% systematic uncertainty is used for 1L and 0L analysis respectively. Figure 6.1 shows the exclusion curve obtained using 1L analysis with Higgs requirement (magenta curve) and using 0L analysis (black and blue curves). The black contour shows the exclusion potential using only baseline selections and the blue contour shows the enhancement in excluding stop mass on using the Higgs information.

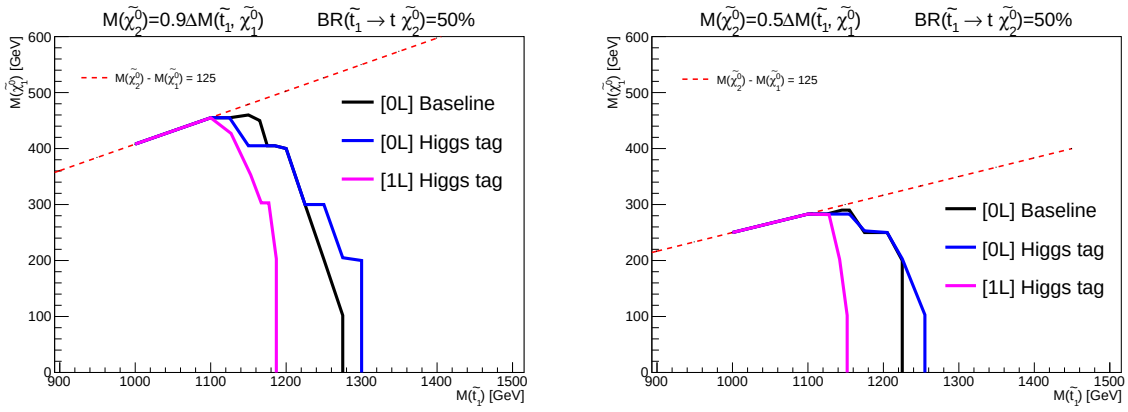

Figure 6.1: Exclusion limit curve for 0.9 (left plot) and 0.5 (right plot) mass fraction and 50% branching ratio for single lepton analysis with Higgs tagging (magenta), fully hadronic analysis with baseline (black) and with Higgs tagging (blue).

The region below the curve is excluded by the analysis and the region outside the curve is not sensitive to this analysis. Note that single lepton analysis exclusion might be further improved by reducing the dilepton $t\bar{t}$ background. Observe that 1L analysis has a lower MET threshold (120 GeV) than 0L analysis (200 GeV) which gives a much cleaner signature. Using a 200 GeV cut on dilepton $t\bar{t}$ background and keeping all other baseline selections, the event yield reduces from 7465 (MET$\geq$120 GeV) to 2790 (MET$\geq$200 GeV) giving a 63% reduction.

It is also found that using an isolated track (not passing the good lepton selection) selection to reject backgrounds reduces the dilepton $t\bar{t}$ contribution by a factor of 2. This study is done on CMSSW dilepton $t\bar{t}$ sample where the isolated lepton tracks are tracks which failed the identification and isolation requirements, and are not a part of the PF lepton categories. This was not simple to implement in Delphes, hence we used CMSSW generated sample, where the conditions used are that of 1L and zero isolated electron or muon tracks.

Thus, using higher MET threshold and vetoing isolated tracks can reduce the $t\bar{t}$ dilepton events which is dominant background source in 1L channel. This can in turn improve the performance of the 1L analysis and be comparable to 0L analysis.

Chapter 7

Summary

Supersymmetry is one of the most studied extension of Standard Model which resolves some of the shortcomings of the SM. It predicts partner particle for every SM particle whose masses and coupling with other particles are unknown, making them the free parameters of the theory. There are various dedicated searches for SUSY particles in a variety of final states targeting diverse model scenarios. There is strong motivation to search for supersymmetric partner of SM top quark in the experiments as it helps stabilize the divergent correction to SM Higgs mass.

In this thesis, we targeted models of stop pair production which decays to top quark via the lightest ($\tilde{\chi}_1^0$) or next to lightest neutralino ($\tilde{\chi}_2^0$). The $\tilde{\chi}_2^0$ is assumed to decay to Higgs boson and $\tilde{\chi}_1^0$. These models are not extensively studied at the CMS experiment and can have a potential to improve the current searches.

Two final state signatures are studied and compared, single lepton channel (1L) and fully hadronic channel (0L). Baseline selections are used to reduce significant amount of background events but maintain signal events as much as possible. For the 1L channel, it is found that M_T cut reduces significant amount of semileptonic $t\bar{t}$ events, leaving dileptonic $t\bar{t}$ process as the major background. For 0L channel, the high MET reduces the QCD background to a large extent. Using multiple b-jets selection reduces the other backgrounds like Z+Jets and W+Jets, leaving $t\bar{t}$ process as the dominant background. The 1L analysis can be further improved by using a higher MET threshold and using isolated track veto to reduce the dominant $t\bar{t}$ dilepton background and hence enhance the sensitivity.

The kinematics of the particles in the event depends on the mass spectra of the SUSY particles. We studied three scenarios defined by $M(\tilde{\chi}_2^0) = x\ \Delta M(\tilde{t}_1,\ \tilde{\chi}_1^0)$ and x=0.9, 0.5, 0.2 giving high, moderate and low p_T Higgs in the event respectively. For scenarios with x=0.9 and 0.5, the Higgs is boosted and its decay products are collimated. The analysis is designed to target the boosted Higgs particles and reconstruct them in a single AK8 jet (Fat Jet). Soft drop tagger and N-subjettiness variable is used to tag the Higgs Fat Jet along with $p_T \geq$300 GeV and $|\eta| \leq$2.4. To have some sensitivity to the models with low p_T Higgs (x=0.2 scenario) and where $H \to b\bar{b}$, we reconstruct the Higgs using a system of two b-jets whose invariant mass lies in Higgs mass window (Resolved Jet) when no Fat Jets are found in the event. These two categories are then combined statistically which give a better sensitivity.

The signal and background events are scaled to their cross-section at 13 TeV and a luminosity of 150 fb^{-1} is used. Higgs Combine Tool is used to calculate upper limits on r-values at 95% confidence level. MC statistical uncertainty is used and 20% and 50% systematics is used for 1L and 0L analysis respectively. It is found that adding a Higgs requirement enhances the sensitivity of the 1L analysis by a large amount, whereas the 0L analysis, being an inclusive analysis has good sensitivity to the stop signal models and adding Higgs requirement improves it only by a small amount. It is also found that 0L analysis is sensitive to a range of branching ratio of $\tilde{t}_1 \to t\tilde{\chi}_2^0$ decay except for the compressed (x=0.2) scenario.

We conclude that Higgs tagging has the potential to improve the traditional searches for stop models and we can hope to see some exciting new physics with more SUSY searches to come!

Bibliography

[1] Abdus Salam & John Clive Ward, Weak and electromagnetic interactions, Phys. Lett. 13, 168-171 (1964), doi: 10.1007/BF02726525

[2] Csaba Csaki & Philip Tanedo, Beyond the Standard Model, Lectures at the 2013 European School of High Energy Physics, arXiv:1602.04228 [hep-ph]

[3] https://cosmosmagazine.com/physics/particle-physics-a-primer-to-the-theory-of-almost-everything

[4] Stephen P. Martin, A Supersymmetry Primer, arXiv:hep-ph/9709356

[5] https://arstechnica.com/science/2014/04/a-sort-of-particle-free-supersymmetry-found-in-exotic-materials/

[6] https://www.quantumdiaries.org/2012/07/01/the-hierarchy-problem-why-the-Higgs-has-a-snowballs-chance-in-hell/

[7] Peter W. Higgs, Broken Symmetries and the Masses of Gauge Bosons, doi: 10.1103/PhysRevLett.13.508.

[8] CMS Collaboration, Observation of a new boson at a mass of 125 GeV with the CMS experiment at the LHC, arXiv:1207.7235 [hep-ex]

[9] ATLAS Collaboration, Observation of a new particle in the search for the Standard Model Higgs boson with the ATLAS detector at the LHC, arXiv:1207.7214 [hep-ex]

[10] https://www.quantumdiaries.org/2012/7/page/6/

[11] Z. Gtschow , Z. Marshal, Setting Limits on Supersymmetry Using Simplified Models, doi:10.3791/50419

[12] CMS Collaboration, Interpretation of searches for with simplified models, doi:10.1103/PhysRevD.88.052017 arXiv:1301.2175.

[13] Barbara Clerbaux, Highlights on searches for supersymmetry and exotic models, Comptes Rendus Physique 16 (2015) 407-423 ScienceDirect (2015-05), doi: 10.1016/j.crhy.2015.04.007.

[14] Search for top squark pair production in pp collisions at $\sqrt{s}$ =13 TeV using single lepton events [arXiv:1706.04402 [hep-ex]].

[15] https://twiki.cern.ch/twiki/bin/view/CMSPublic/PhysicsResultsSUS

[16] https://twiki.cern.ch/twiki/bin/view/AtlasPublic/SupersymmetryPublicResults

[17] ATLAS Collaboration, Search for direct top squark pair production in events with a Higgs or Z boson, and missing transverse momentum in s = $\sqrt{13}$ TeV pp collisions with the ATLAS detector, J. High Energ. Phys. 2017, 6 (2017), arXiv: 1706.03986

[18] https://home.cern/science/accelerators/large-hadron-collider

[19] CMS Collaboration, The CMS Experiment at the CERN LHC, JINST 3 (2008) S08004, doi: 10.1088/1748-0221/3/08/S08004

[20] http://inspirehep.net/record/913551/plots

[21] Tejinder S. Virdee, Experimental Techniques

[22] CMS Collaboration, Particle-flow reconstruction and global event description with the CMS detector, JINST 12 (2017) P10003, doi: 10.1088/1748-0221/12/10/P10003 arXiv:1706.04965 [physics.ins-det]

[23] http://inspirehep.net/record/884672/plots

[24] Arthur Alexis Jules Lesage, Lepton and photon performance at ATLAS and CMS, ATL-PHYS-PROC-2017-123, arXiv:1709.02598 [hep-ex]

[25] Ryan Atkin, Review of jet reconstruction algorithms, 2015 J. Phys.: Conf. Ser. 645 012008

[26] M. Cacciari, G. P. Salam, and G. Soyez, The anti-k t jet clustering algorithm, JHEP 0804:063 (2008) doi:10.1088/1126-6708/2008/04/063 arXiv:0802.1189.

[27] CMS Collaboration, Identification of b-quark jets with the CMS experiment, JINST 8 (2013) P04013, doi: 10.1088/1748-0221/8/04/P04013 arXiv:1211.4462 [hep-ex]

[28] https://en.wikipedia.org/wiki/B-tagging

[29] https://twiki.cern.ch/twiki/bin/view/LHCPhysics/SUSYCrossSections13TeVstopsbottom

[30] J. Alwall et al. arXiv:1405.0301, JHEP 1407 (2014) 079

[31] T. Sjstrand, S. Mrenna and P. Skands, JHEP05 (2006) 026, Comput. Phys. Comm. 178 (2008) 852.

[32] J. de Favereau et al. [DELPHES 3 Collaboration], JHEP 1402 (2014) 057 doi:10.1007/JHEP02(2014)057 arXiv:1307.6346 [hep-ex]

[33] M. Cacciari, G.P. Salam and G. Soyez, Eur.Phys.J. C72 (2012) 1896 [arXiv:1111.6097]

[34] Rene Brun and Fons Rademakers, ROOT - An Object Oriented Data Analysis Framework, Proceedings AIHENP'96 Workshop, Lausanne, Sep. 1996, Nucl. Inst. & Meth. in Phys. Res. A 389 (1997) 81-86. See also http://root.cern.ch/

[35] J. Butterworth, A. Davison, M. Rubin, G. Salam, Jet substructure as a new Higgs search channel at the LHC, doi: 10.1103/PhysRevLett.100.242001 arXiv:0802.2470 [hep-ph]

[36] A. Larkoski, S. Marzani, G. Soyez, J. Thaler, Soft Drop, doi: 10.1007/JHEP05(2014)146 arXiv:1402.2657 [hep-ph]

[37] Jesse Thaler, Ken Van Tilburg, Identifying Boosted Objects with N-subjettiness, JHEP 1103:015,2011, doi: 10.1007/JHEP03(2011)015 arXiv:1011.2268 [hep-ph]

[38] $https://cds.cern.ch/record/2257107/files/ATL-PHYS-SLIDE-2017-110.pdf$

[39] $https://msneubauer.github.io/projects/4_project/$

[40] $https://indico.in2p3.fr/event/16354/contributions/59512/attachments/49415/62820/Lecture_2018$

[41] A. L. Read, Presentation of search results: The CL(s) technique, J. Phys. G 28 (2002) 2693, doi:10.1088/0954-3899/28/10/313

[42] The ATLAS Collaboration, The CMS Collaboration, The LHC Higgs Combination Group Procedure for the LHC Higgs boson search combination in Summer 2011.

[43] http://twiki.ihep.ac.cn/twiki/view/CMS/CombineTutorial

[44] https://wiki.physik.uzh.ch/cms/limits:limits#simple_examplerunning_the_combine_tool

[45] GEANT4 Collaboration, GEANT4 a simulation toolkit, Nucl. Instrum. Meth. A 506 (2003) 250, doi:10.1016/S0168-9002(03)01368-8.

[46] CMS Collaboration, Search for direct production of supersymmetric partners of the top quark in the all-jets final state in proton-proton collisions at $\sqrt{s} = 13$ TeV, doi:10.1007/JHEP10(2017)005 arXiv: 1707.03316 [hep-ex]

[47] CMS Collaboration, Search for supersymmetry in proton-proton collisions at 13 TeV in final states with jets and missing transverse momentum, doi:10.1007/JHEP10(2019)244 arXiv: 1908.04722 [hep-ex]